Removal of Mercury Vapour from Fluorescent Lamps Using Activated Carbonaceous Material from Waste Tyre Pyrolysis

MSc Environmental Engineering Research Report

Prepared by:

Delford Dovorogwa
Student Number: 1481405

A research report submitted to the Faculty of Engineering and the Built Environment, University of the Witwatersrand, Johannesburg, in partial fulfilment of the requirements for the degree of Master of Science in Engineering

Supervisor: Professor Sunday Nwaubani
Co-Supervisor: Professor Michael Daramola

September 2020

DECLARATION

I declare that this research report is my own unaided work. It is being submitted to the degree of Master of Science in Engineering to the University of the Witwatersrand, Johannesburg. It has not been submitted before for any other degree or examination in any other University.

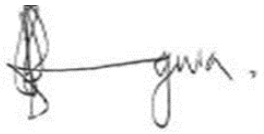

Delford Dovorogwa

18th day of __SEPTEMBER___ 2020

DEDICATION

In memory of my late grandmother (*Mbuya vaHondo, Nee E. Dzani*). You truly showed us the full meaning of love in Christ Jesus. May your soul rest in peace. To my parents, you are my living heroes. To my daughters, Taropafadzwa Faithful and Tawananyasha Faith and to my beloved wife Stella, girls this is all for you.

ABSTRACT

Elemental mercury, its vapours in the environment or in it's bioaccumulated forms within seafood as well as plants destined for human consumption poses health challenges. In this study, removal of mercury vapours from end-of-life flourescent lighting waste using adsorption technology was investigated. The objective was to establish if, carbon black from the pyrolysis of waste tyres could be exploited for use as mercury adsorbent during recycling of flourescent lamps. Two portions of the pyrolitic carbon black were separately activated using sulphuric acid (H_2SO) and hydrogen peroxide (H_2O_2). These carbons' adsorptive potential were evaluated against that of commercially available activated carbon. The tyre pyrolytic carbon was characterised before activation, after activation and after adsorption trials to evaluate the adsorptive potentials. This characterisation included Fourier-Transform-Infra-Red spectroscopy, Scanning Electron-Microscopy coupled with Energy Dispersive X-ray, Brunauer-Emmet-Teller and powder X-ray Diffraction techniques. The adsorption testing trials involved thermal generation of mercury vapours which were then passed through an adsorbent packed column reactor while exiting through an outlet on the other end of that reactor. This vapour flow across the reactor proceeded for a fixed duration before the adsorbent was qualitatively checked for any mercury adsorption on its surfaces. Raw pyrolytic carbon black, showed some adsorption promoting functional groups which quantitatively improved after both sulphuric acid and hydrogen peroxide activation. Morphology tests based on SEM technique revealed that the porosity of acid activated carbon and the peroxide activated carbon were both fourteen times more than that of the raw pyrolytic carbon black. Adsorption of mercury on activated pyrolytic carbon surfaces was observed although this was less intense when compared to that on the commercial activated carbon. The adsorptive perfomance of activated pyrolytic carbon black was encouraging, demonstrating its technical potential in elemental mercury adsorption. The hydrogen peroxide activated carbon was superior compared to the sulpuric acid activated with mercury recoveries of 92% and 90% respectively.These recoveries are however lower than that of other previously studied corn based activated carbon which were above 98% in other cases according to literature. It is therefore recommended to carry out indepth adsorption optimisation studies targeting tyre based carbon improvements to match or exceed the perfomance of other activated carbon.

ACKNOWLEDGEMENTS

First, I would like to express my gratitude to the Almighty God for the sufficiency of his grace which enabled me to complete this study. I thank all who in one way or the other contributed to the successful completion of this study.

I am much indebted to my Supervisors, Professors Sunday Nwaubani and Michael Daramola for their understanding, guidance and intellectual criticism during the execution of this research study. I must acknowledge with gratitude my Supervisors' patience, moral support and special interest in the success of the execution of this project.

My project would not have been complete without the help and assistance of my Laboratory Supervisor, Dr M. Matandabuzo. You are an amazing person. Thank you for all the huge amount of time and effort you spend with me. I feel privileged to find in you, a brother and a friend at the end of this study.

I would also want thank Charles Rashama, a colleague, who helped me with the proofreading of this report.

At last but not the least, my heart felt gratitude goes to my wife Stella, my lovely angels, Taropafadzwa Faithful and Tawananyasha Faith, for their unwavering support during the whole period of this research study. I have no valuable words to express my gratefulness, but the three of you together, are the pillar of my strength. You always give me another good reason to wake-up with renewed strength every other day.

TABLE OF CONTENTS

LIST OF SYMBOLS

Å - Angstrom

a - effective cross-sectional area of one adsorbate molecule in m^2

c - Concentration of Hg vapour in p, g/m3,

C - Dimensionless constant that is related to the enthalpy of adsorption of the adsorbate gas

cc - is the polarization constant.

H_2O_2 - Hydrogen peroxide chemical formula

H_2SO_4 - Sulphuric acid chemical formula

H_3PO_4 - Orthophosphoric acid

k - Experimentally determined constant

m - mass of test powder, in grams

m - Mass of the adsorbent in g,

n - Experimentally determined constant

N - Avogadro constant (6.022×10^{23} mol^{-1}),

P - Partial vapour pressure of adsorbate gas in equilibrium

Po - Saturated pressure of adsorbate gas, in pascals

Rr - reflectance (amplitude) of the beam splitter,

S_{BET} - BET surface area

Tt - is the transmittance, and

Va -Volume of gas adsorbed at standard temperature and pressure (STP)

Vm - volume of gas adsorbed at STP to produce an apparent monolayer on the sample surface.

X - Amount of Hg vapour adsorbed in micrograms

Δd - is the path difference,

LIST OF FIGURES

LIST OF TABLES

LIST OF ABBREVIATIONS

AC	- Activated Carbon
aCB	- Activated Carbon Black
ASTDR	- Agency for Toxic Substances and Disease Registry
BET	- Brunauer-Emmet-Teller
CB	- Carbon Black
CFL	- Compact Fluorescent Lamps
COP	- Conference of Parties
DSM	- Demand Side Management
EIA	- Environmental Impact Assessment
EPA	- Environmental Protection Agency (of USA)
E-WASA	- e-Waste Association of South Africa
FTIR	- Fourier Transform Infrared
IEEE	- Institute of Electrical and Electronics Engineers
IMERC	- Interstate Mercury Education and Reduction Clearinghouse
ISO	- International Organisation of Standardisation
JMAJ	- Japan Medical Association Journal
kWh	- Kilo Watt Hour
LED	- Light Emitting Diode
LFT	- Longitudinal flourescent tube
NARAP	- The North American Regional Action Plan
NEES	- National Energy Efficiency Strategy
PDCA	- Plan Do Check Act (Quality Management Principle)
pXRD	- powder X-ray Diffraction
SEM	- Scanning Electron Microscope
TLV	- Threshold Limited Value
UNCSD	- United Nations Commission on Sustainable Development
UNEP	- The United Nations Environment Programme
WHO	- World Health Organisation

CHAPTER ONE: BACKGROUND AND MOTIVATION

1.0 Introduction

The rapidly increasing electricity demand and cost coupled with an extended carbon emission footprint has motivated the South African government to replace the inefficient, high energy demanding incandescent lighting lamps with more efficient lighting technologies. Among these efficient technologies are the compact flourescent lighting lamps (CFLs), the longitudinal flourescent tubes (LFTs) and the light emitting diodes (LEDs). Of these lamp technologies, the CFLs have been widely adopted in South Africa. The National Energy Efficiency Strategy (NEES) of South Africa whose implementation began in 2005, targeted the phasing out of the incandescent light bulbs in an attempt to improve electrical energy utilisation efficiency and decouple economic growth from energy demand. In the Western Cape province, alone, 5 million compact flourescent lamps were distributed over a period of 10 years to replace incandescent bulbs as part of this exercise (Ringwood, 2015). This exercise resulted in a 10% improvement in energy utilisation efficiency within the lighting sector of South Africa in 2015.

When compared to incandescent lights, CFLs use approximately 75% less energy while LEDs use approximately 80% less energy with both lamps also claimed to longer than the incandescent lights (Singh and Katal, 2013). During the last decade, the lighting industry has experienced a massive growth, specifically in the energy efficient flourescent lighting technologies. There has been unprecedented increase in market uptake of these CFLs. This subsequently increases waste generated from the same industry as breakages are formed during production, transportation and mainly at the point of use. While the benefits of using the energy efficient compact flourescent lighting technology were obvious, the concerns regarding their end-of-life management as they contain mercury have been raised. Waste CFLs contain mercury (Hg) which is hazardous to human health when inhaled or ingested. Waste generated from electrical and electronic equipment in 2015 within South Africa amounted to 17 733 tonnes while 4% of this was a contribution from CFLs (Lydall et al., 2017). These numbers are likely to keep increasing annually as efforts to be energy efficient in the lighting industry continue to gain momentum in most countries including South Africa. Ingestion of Hg by human beings can also happen indirectly. This is when one eats fish that has previously survived on seabed muddy and zooplankton. It is in these environments where the Hg normally settles and bioaccumulates after

being washed by surface runoff water. Inhalation of mercury vapours can take place when this volatile metal is heated and then evaporates into the sorrounding atmosphere during the disposal stages of brocken lamps. Mercury is a known neurotoxin and can be dangerous once it is released into the environment. It is a toxic heavy metal that bio accumulates in organisms and causes brain and liver damage if ingested or inhaled by human beings. The efficiency and sustainability of control in managing Hg vapour release from compact fluorescent lamp waste in South Africa, is not adequately documented. Therefore specific studies aimed at developing cheaper and locally available technology to control Hg vapours release is necessary. At first glance the new energy efficient lighting technology appears to be the better way to reduce energy consumption and protecting the environment, however, the serious Hg management concerns associated with use of CFL lamps needs to be considered and addressed. Depending on the type of lamp, a longtudinal compact fluorescent lamp may contain Hg from greater than 0.1 upto 100 milligrams (mg) with 99% of this Hg resident in the phosphor powder and this powder constitute at maximum 2% weight of the lamp (Rhee et al., 2015). Although procedures have been developed for Hg extraction from the wastes during recycling, adequate controls to contain the vapours are not clearly documented. Furthermore adaptation of the technologies to local conditions either for cost reduction or efficiency improvement has not been adequately investigated. To close this gap, adsorption studies will be conducted with locally available waste tyres pyrolytic carbonaceous residues towards capturing mercury vapours.

The automobiles industry has been growing steadily over the past few years and this growth ultimately result in generation of excessive waste tyres. It is estimated that about 1.5 billion waste tyres are produced annually worldwide (Danon et al., 2015). South Africa having stockpiles of exceeding 2 million tonnes (Pilusa et al., 2014) the majority of ends up in landfills. Waste tyres, like rubber, do not readilly decompose, so their disposal come with challenges such as excessive energy consumption. A waste tyre to energy pyrolysis plant operated by a company called Recor in Pretoria, South Africa, produces three products namely, pyrolytic oil, pyrolytic carbon black and a gas fraction (Recor, 2019). The carbon black currently produced at the Recor pyrolysis plant has not found any significant use to justify its production from this plant. This study therefore seeks to investigate the use of carbon black residue from waste tyre pyrolysis as an adsportion agent for the removal of mercury vapour from fluorescennt lamp waste recycling, yet another waste hurdle, the country is grappling on.

Waste tyre pyrolytic carbon was evaluated during this research study for its Hg adsorptive properties hence potential application in mercury recovery. The waste tyre carbon residue used was sourced from waste tyre pyrolysis process by Recor. The other adsorbent used for comparative studies was a commercially available activated carbon collected from Reclite, a fluorescent lamp waste recycling company based in Germiston, Gauteng Province in South Africa. This company, imported the fluorescent lamp recycling plant, including the activated carbon filter cartridges from Sweden. The commercial grade activated carbon was produced and supplied by a Swedish based company specialising in technology and equipment for the safe disposal/recycling of mercury containing waste products.Adsorption, precipitation, and oxidation are some of the well known methods for removal of toxic substances from gases and liquid effluents. Activated carbon is the most commonly used adsorbent but the major drawback of activated carbon is that it is a very expensive material and developing countries, struggle financially to import and utilise activated carbon on large scale operations (Mukosha et al., 2013). Because of this disadvantage, the search for alternative adsorbents continues to top on research agendas. The current research was also motivated by this societal need in the wake of increasing Hg containing wastes from which the mercury must be recovered.

1.2 Problem Statement

A sustainable alternative adsorbent for the recovery of Hg vapour from compact fluorescent lamp waste is needed. Mercury recovery is initiated to mitigate against the health risks associated with mercury disposal into the environment. Currently imported and expensive activated carbon is the adsorbent of choice because of limited locally competing products. On the other hand, waste tyres recycling produces a carbonaceous residue which has no immediate uses in the country though it is anticipated to exhibit adsorptive properties. If waste tyres pyrolytic carbon can be developed for use as an adsorbent, in the recovery of mercury, this strategy would solve two societal problems concurrently. This would probably be a more sustainable Hg management option in the South African context than the use of costly imported adsorbents.

The main research questions for this study are:

a. Can a mercury vapor adsorbent be prepared from the carbonaceous residue of waste tyre pyrolysis?

b. How does tyres pyrolytic carbonaceous material derived adsorbent compare to the currently industry adopted mercury vapour adsorbents?
c. Could the choice of activation agent matter in the preparation of mercury adsorbent from tyre pyrolytic residues?

1.3 Research Aims

The main aim of this research study is to develop a cost-effective locally available mercury vapour adsorbent.

1.4 Research Objectives

The specific objectives of this research are to:

a. Produce activated carbon from pyrolytic carbon black (waste tyre pyrolysis by-product) by sulphuric acid and hydrogen peroxide routes.
b. Evaluate if the activated waste tyres pyrolytic carbon would adsorb mercury vapours.
c. Compare the mercury adsorption potential of activated pyrolytic carbon black to that of the currently used commercial product.

1.5 Research Report Layout

The first chapter in this report, the Introduction, shall outline the research background, highlighting the motivation behind this research. A brief account of how and why the lighting industry uses the CFLs is given. The health issues regarding mercury in these lights posing challenges on lamp disposal are discussed. The research problem statement, aim and objectives are formulated and stated in this introductory chapter. Detailed literature survey on mercury toxicity and technologies for mercury management with emphasis on adsorption will be carried in chapter two. The methods and techniques that will be used in this research study shall be described in chapter three. Chapter 3 will therefore also give a detailed account of the various adsorbent analytical techniques used including Fourier transform infrared spectroscopy (FTIR), scanning electron microscopy/energy dispersive X-ray spectroscopy (SEM/EDX), powder X-ray diffraction (pXRD) and Brunnauer Emmett-Teller methods (BET). Experimental results and their discussion will be reported under chapter four with the final chapter (Chapter five) stating the research conclusion and recommendations

CHAPTER TWO: LITERATURE SURVEY

2.0 Chapter Overview

This chapter reviews literature related to mercury in fluorescent lighting and electronic waste regulations in South Africa. Specific issues reviewed include the adoption of fluorescent lighting in South Africa, fluorescent lighting principles, the toxicity of mercury, recovery of mercury from fluorescent lighting waste, South African regulations on e-waste, adsorption and adsorbent materials for mercury vapour recovery then adsorption principles in gases and liquids. An account is also given of how analytical techniques necessary for adsorption studies work covering SEM, BET, pXRD and FTIR.

2.1 The Adoption of Fluorescent Lighting in South Africa

The price of electricity has increased tremendously in South Africa over the past decade. Around 2009, one kWh unit of electricity was costing R32.72 c/kWh compared to the 2019 rate of R116.76 c/kWh (Eskom, 2019). The continued rise in electricity demand, escalation in costs and extended carbon emission footprint has forced the government of South Africa, to look for ways to manage these challenges mainly by addressing utilisation efficiency in different sectors of the economy. One of the solutions previously implemented by the government was to replace incandescent lights with emerging energy efficient lamp technologies such as the CFLs. The first use of CFLs in South Africa was introduced as a Demand Side Management (DSM) initiative called BONESA in 1999. The initiative was part of National Energy Efficient Strategy for South Africa and was jointly funded by the Global Environmental Facility and Eskom (Tiedemann et al., 2004). Some of the implementation strategies used in this initiative included customer education, advertising and marketing. The second phase of this initiative came on board around 2005 and its main aim was the phasing out of incandescent light bulbs to reduce the nation's energy intensity and decouple economic growth from energy demand. According to Ringwood (2015), more energy DSM programs were rolled out between 2005 and 2015 and in the Western Cape province, alone, 5 million CFLs were distributed. As a result of these programs an overall 10% improvement in energy efficiency within the lighting sector was achieved by 2015.

2.2 Fluorescent Lighting Principle and Mercury

The construction and operating principle of a CFL is described by Singh and Katal (2013). The CFLs consist of a glass tube with electrodes, filled with a gas and a little amount of Hg. The glass wall is coated inside with a phosphor layer, as seen in Fig 2.1. The CFL converts invisible radiant energy into visible light of longer wavelength. Firstly, a voltage is applied to the two electrodes of the lamp and this triggers a gas discharge between the electrodes. Electrons are accelerated in the field generated by the electrodes and these excite the atoms of Hg gas onto a higher energy level. When these atoms subsequently return to their original level, they give off this difference in energy - mostly in the form of photons of ultraviolet radiation. This causes the emission of invisible light. This invisible light is then converted into visible light by the phosphor layer on the glass tube. This working principle of CFL is very energy efficient resulting in CFLs consuming 80% less energy than their incandescent counterparts (Singh and Katal, 2013) for the same light output. Additionally, CFLs have a longer life span than the incandescent lights. These attributes promoted rapid adoption of CFLs as replacements of incandescent lights on the market as explained previously. The increasing usage of CFLs greatly and positively reduced the uneconomic consumption of electricity hence indirectly reduced carbon emissions also especially in South Africa where the greater portion of electricity is generated from the combustion of coal. However, the CFLs contain Hg as a functional component of the light bulbs. The health risks associated with exposure to Hg are widely documented (Beckers and Rinklebe, 2017; Kim et al., 2016). Compact fluorescent lamps end-of-life wastes are therefore included in the range of electrical and electronic waste (e-waste) which is classified by international convention (Basel Convention – Annexure 1) as hazardous waste (Choi et al., 2020). The phosphor powder found in fluorescent lights is composed of various combinations of naturally fluorescing minerals such as willimite phosphor (Mn^{2+}-activated Zn_2SiO_4); calcium halo phosphate phosphor ($Sb^{3+,}$ Mn^{2+}-activated $Ca_5(PO4)_3(ClF)$ (Xia and Meijerink, 2017). Although fluorescent lamps come in different shapes and sizes, they all contain the health risk from Hg to different extents, hence their disposal motivated for this study. Standard straight lamps typically contain <10 mg mercury per unit, with newer tri-phosphor lamps containing <5 mg while other lamp types may contain higher levels of mercury (Tan and Li, 2016). Mercury is slowly absorbed into the glass phosphor powder and electrodes throughout the lamp's life. Mercury will, therefore, be unevenly distributed throughout the lamp (Rhee et al., 2015).

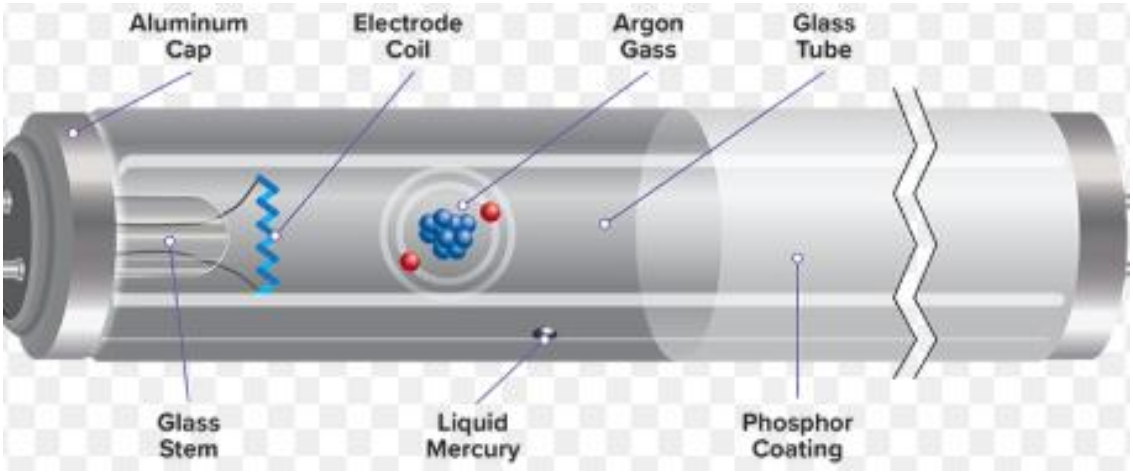

Fig 2.1: Structure depicting a compact fluorescent lamp. Source: *(Duncan, 2019)*

Any uncontrolled breakage of the lamps results in the discharge of the mercury vapour into the environment. Mercury assays of as high as 700 mg/kg of dry waste of broken CFLs have been reported in literature (Tunsu et al., 2014).

2.3 Health Concerns Related to Mercury

Mercury is well documented as one of the most toxic yet widely used heavy metal in various industries (Horowitz et al., 2014). Mercury is a neurotoxin and can be dangerous once it is released into the environment. Mercury vapour is invisible and odourless and can readily vaporise even at ambient temperatures. Mercury can be environmentally transformed into methylmercury which bioaccumulates in living organisms and is highly toxic. Elementary Hg vaporises (sublimes) at room temperature and in this form, it be easily inhaled.

The mechanisms of Hg toxicity are well documented elsewhere (Carocci et al., 2014; Ynalvez et al., 2016). Mercury as a heavy metal bio accumulates in organisms and causes brain and liver damage if ingested or inhaled by human beings. Mercury poisoning is known as hydragaria or mercurialism and this happens exposure to Hg and/or its compounds. When Hg vapour is inhaled, its lipid-soluble property allows for easy passage through the alveoli into the blood stream and red blood cells. Non-oxidised elementary Hg in the blood stream penetrates the central nervous system where it is ionised and trapped. Acute exposure caused by inhalation of elementary Hg can lead to pulmonary symptoms. Initial signs and symptoms include fever, chills, short breaths and pleuric chest pains. Organic mercury is found in three forms, aryl, short and long chain alkyl compounds, (Lohren et al., 2015). They are absorbed completely from the

gastrointestinal tract because they are lipid soluble and mildly corrosive. Once absorbed, they are converted to the inorganic form and possess similar toxic effects as inorganic Hg. Methylmercury has a high affinity for sulfhydryl groups which contributes to its effects on enzyme dysfunction (inhibition). It inhibits the enzyme choline-acetyltransferase involved in the final step of acetylcholine production, leading to acetylcholine deficiency (Yoshida et al., 2016).

People can be exposed to Hg directly from products containing elemental Hg and indirectly through ingestion of seafood, or other crops in which Hg has bioaccumulated in the form of methylmercury (Maroneze et al., 2014). Another route is through inhalation. This can happen when the Hg is containing products are warmed and the Hg vaporises in poorly ventilated warm spaces. Mercury vaporises (sublimates) at room temperature and is highly absorbed through inhalation (Maqbool et al., 2017). With thousands of bulbs sold and distributed around South Africa and inadequate disposal facilities, a Hg time bomb could be in the making. Mercury can be released into the environment if the lamps are accidentally broken at recycling facilities when the vacuum systems that control Hg escape are not functioning well or when Hg containing waste is disposed at a landfill site. Emissions resulting from end of life treatment of the CFLs may release other hazardous compounds into the environment, such as dioxins and furans. Compact fluorescent lighting lamp waste requires specific and efficient management to ensure proper containment of these toxic components.

2.3.1 Historical incidences of mercury toxicity

Minamata disease, which is a distinctive example of the mercury pollution related effects to human health and the environment was reported in 1956 and occurred in the Minamata Bay, Kumamoto, Japan. Mercury contamination in Japan's Agano river basin, Nigata, re-ocurred in 1965 (Yorifuji and Tsuda, 2016). The causal substance in the Minamata incident was methylmercury which was produced as a by-product of acetaldehyde discarded from Chisso Corporation into Minamata Bay and from Showa Denko Company into the Agano river basin. The released methylmercury from both factories bioaccumulated and biomagnified heavily in fish and sea food which was the main source of food for the local people. Later on, the mercury poisoning manifested in human beings as an illness referred to as Minamata disease. The signs and symptoms of the Minamata disease patients included sensory disorders, disturbance in the distal portions of four extremities, ataxia, concentric contraction of the visual field, etc (Puty et

al., 2019). The lessons learnt from the Minamata incident was that the environment should never be compromised for economic gains.

In Iraq, Hg pollution and poisoning occurred twice, in the 1970s when large numbers of people from small villages consumed seed grain that had been treated with fungicides containing alkyl mercury compounds (Honda et al., 2006). The first incident was caused by ethlymercury treated grain and adversely affected about 1000 people. The second incident was caused by seed grains treated with Hg after the planting season which were later used to make flour for human consumption through bread making. From this incident, about 6500 patients were hospitalised, and 459 deaths were recorded mainly due to failure of the central nervous system. The toxicity was observed in many adults and children who had consumed the bread over a three-month period. The greatest effects were observed among off springs of pregnant women who ate the contaminated bread during their pregnancy. Infants born to mothers who had eaten the bread exhibited symptoms ranging from delays in speech and motor development to mental retardation, reflex abnormalizes and seizures.

2.4 Regulations Regarding E-waste in South Africa

South Africa faces several recycling management challenges related to e-waste and generally there is lack of basic health, safety and environmental precautions at some waste handling sites. The handling of e-waste is mostly informal and covers the early stages of recycling, (i.e. – collection, crude dismantling and sorting). These informal recyclers are vulnerable as they are often directly exposed to the hazardous components of the e-waste (Bob et al., 2017).

Mercury from CFL technology has been grouped under hazardous general household waste streams (Venter, 2008). Key issues with this waste include inadequate waste collection, illegal dumping, unlicensed waste management activities, insufficient waste minimisation and recycling activities as well as lack of waste information and legislation enforcement. Notwithstanding the comprehensive guidelines prepared by Eskom (Eskom, 2013), some of the challenges in the efficient management of hazardous e-waste are still attributed to the absence of both the recycling infrastructure and legal framework. The regulatory institutional framework on waste management has been reactive towards the management of potential impacts associated with the CFL lamp waste. In 2013, a review of the Waste Management and Classification Regulations (R364), introduced aspects of waste classification and management. However, the review lacked

coverage on hazardous substances such as Hg contained in the CFLs. The legislation did not define or prescribe the minimum and specific requirements for the monitoring of potential Hg release during storage, transportation treatment and or recycling of CFL lamp waste. Several laws that address waste management in South Africa contain sections covering e-waste handling. Some of these laws and regulations are the National Environmental Management Waste Amendment Act, 26 of 2014, the National Waste Management Strategy (Department of Environmental Affairs, 2012), National Environmental Management Act, 107 of 1998 (NEMA, 1998), Environmental Conservation Act (Environmental Conservation Act No.73 of 1989), Hazardous Substances Act (Hazardous Substances Act, 1973). National Water Act, 36 of 1998 (National Water Act, 1998), Atmospheric Pollution Prevention Act, 45 of 1965 (Atmospheric Pollution Prevention Act, 1965), and Occupational Health and Safety Act, 86 of 1993 (Occupational Health and Safety Act, 1993). These laws are however disjointed as their superintendent falls under different jurisdictions. Sometimes officials from the different government departments fight for control or come with contrasting approaches to waste management complicating the e-waste regulatory environment (Ghosh et al., 2016). The lack of proactive approach by the regulatory institutional authorities in addressing waste management challenges brought about by the ever-changing technological requirement is resulting in the waste management sector suffering from pervasive under-pricing. This is a situation where the cost and value of waste management is not fully appreciated by consumers and industry, and results in preferential waste disposal on landfills over other options (Oyekale, 2015). According, to Panchia and Krige (2020) estimates put the number of waste handling pickers at 90 000 individuals in South Africa and around 2 000 waste handling facilities, however a significant number of these are not licensed. This calls for policy measures to put systems in place for proper monitoring and management of uncontrolled release of Hg from CFL lamp waste at the points of use, storage, transportation as well as the recycling and treatment facilities.

2.5 Studies on Mercury Recovery from Waste Streams

Mercury can be driven out from mine wastes by heating the wastes to temperatures above 400^{o}C using rotary kilns employing fuel or solar heating. Recoveries greater than 90% have been reported by this simple thermal technique (Navarro et al., 2014). Once mercury is converted to vapour form, it can now be adsorbed on a suitable adsorbents such activated carbon, fly ash, biochars, diatomite, zeolitic nanomaterials, etc prior to recovery by desorption (Jampaiah et al.,

2016; Liu et al., 2019; Xu et al., 2019). In using these adsorbents metals, sulphur, metal sulphites or oxides are normally included as active components that improve the adsorptive behaviour of different materials (Abai et al., 2015). Liquid scrubbing with sodium hypochlorite solution has been reported as an effective mercury recovering technique for mercury in flue gases. Hypochlorite leaching of HgS ores has been used to take Hg into solution as $HgCl_2$. Continuous recycling of the leaching solution causes Hg concentrations to increase until all the chloride is converted to $HgCI_2$. At this point, continued addition of elemental Hg causes the reduction of $HgCl_2$ to insoluble HgCI that can be removed by solids-separation methods. Scrubbing of Hg vapours with sodium hypochlorite solution was shown to be ineffective for removing Hg from the kiln off gases (Tunsu et al., 2014). It has been established that mercury in rotary-kiln off gases can be captured on activated charcoal adsorbers while maintaining exit concentrations of 0.005 mg Hg/m^3 or even <0.002 mg Hg/m^3. It is presumed that because of high Hg vapor pressure at room temperature and the tendency of many if not all carbonaceous materials to adsorb Hg, exposure concentration limits required by OSHA regulations for an 8-hour workday can be achieved. Thermal retorting and thermal-desorption processing of Hg-containing materials is inherently a process requiring both low-capital and low-energy consumption that can produce, in most circumstances, a nearly pure Hg product by condensation.

The United States of America's Department of Energy (DoE)'s Transuranic and Mixed Focus Area (TMFA) is responsible for investment into cutting edge technical and engineering solutions for transuranic and mixed waste characterisation and processing for shipment and disposal. It compared possible several Hg treatment technologies on a variety of waste streams. These emerging technologies were expected to have the following attributes:

- Minimize worker exposure
- Minimize volume of waste destined for long-term storage
- Minimize secondary waste generation and
- Maximize operational flexibility and radionuclide containment.

Four technologies each from Brookhaven National Laboratory (BNL), Nuclear Fuel Services, Inc. (NFS), Allied Technology Group (ATG), and the SepraDyne Corporation (through its subsidiary Raduce, Inc.) were investigated. The Sulphur Polymer Stabilization/Solidification (SPSS) process was offered by NBL while NFS technology is called DeHg process. The

technology from ATG also employed chemical stabilization principles with proprietary formulations. A vacuum thermal retorting technique was demonstrated by SepraDyneÔ-Raduce. Each of the first three participants was successful in their respective demonstration mainly in the stabilization of mixed waste containing total Hg greater than 260 ppm to provide data on the applicability of stabilization to high Hg content waste. Three comparative studies showed that the SepraDyneÔ-Raduce process removed total Hg to levels ranging 2-8 ppm and leachable Hg to 0.008 mg/L or less. In addition, because of the very low total volume of gases emitted, the total mass of Hg emitted to the atmosphere during these demonstrations was negligible.

It has been reported recently that Honeywell UOP, a company based in the United States of America has made recent advances in low level Hg detection, which finds use in the petrochemical hydrocarbon refinery feed streams. They developed a regenerative Hg removal adsorbent (HgSIV) which achieves both products drying as well as Hg removals to less than 0.01 micrograms per normal cubic meter. Since the sorption sites for Hg removal are separate from and additive to the dehydration sites in this adsorbent, Hg removal is accomplished by replacing a portion of the dehydration grade molecular sieve with HgSIV adsorbents. The dryer bed size does not have to be increased to remove both water and Hg. Hydrocarbon process stream dryers containing HgSIV adsorbents have the same performance and lifespan as typical molecular sieve dryers. The removal of Hg is completed from HgSIV adsorbents at conventional dryer regeneration temperatures. Properly regenerated HgSIV adsorbents can be disposed of as non-hazardous waste. Hg can be removed from the regeneration gas by condensation when the Hg level in the feed gas is high. Treatment of the HgSIV spent regeneration gas is usually not needed for low to moderate Hg feed gas levels.

2.6 Mercury Recovery Through Adsorption

2.6.1 The adsorption process

The phenomenon of Hg vapour sorption is well studied and documented as a Hg recovery option. Gases such as Hg vapour adsorb onto solid material surfaces due to weak van der Waals forces (Kawai et al., 2016). Sometimes, molecular-sized pores serve as molecular traps, and in other cases, weak electrostatic forces operate at the surface. Adsorption is therefore a reversible process and will continue until equilibrium conditions are established between the vapour phase and the solid phase whereby the adsorption sites will be saturated resulting in an equal rate of

adsorption and desorption. Adsorption mimics dissolution in some respects though the latter takes place on the surface only. The solubility of one material into another is generally governed by the rule "like dissolves like." Mercury vapour exists as a nonpolar molecule that would likely be most soluble in nonpolar substances such as other metals and nonpolar hydrocarbons. Various materials have been shown to adsorb Hg vapour by either physical or chemical mechanisms. Chemical chemisorption involves much stronger forces such as electrostatic which are beyond the van der Waals forces (Moerz and Huber, 2014). The adsorption behaviour of Hg on various materials can be described by adsorption isotherms, which relates the vapour pressure of the adsorbed species to vapour concentration. The most popular among many of these relationships is the Freundlich adsorption isotherm which is mathematically represented as in Equation 1:

$$\frac{x}{m} = kC^n \dots\dots\dots\dots\dots\dots\dots\dots\dots\dots\dots\dots\dots\dots\dots\dots\dots\dots\dots\dots\dots\dots\dots\dots\dots\dots (1)$$

Where x = amount of Hg vapour adsorbed in micrograms,

m = mass of the adsorbent in g,

C = concentration of Hg vapour in g/m^3,

and **n** and **k** are experimentally determined constants.

Thermal desorption is the reversal of the adsorption process by addition of heat. The critical factors affecting the efficiency of the thermal Hg desorption are the Hg vapour pressure and mass transport in the vapour phase. At low temperatures and low vapour pressure, the Freundlich isotherm usually shows a linear relationship between vapour pressure and adsorbed concentration. However, as adsorbed concentrations approach the solubility limits or adsorption capacity of the adsorbent, the slope of the isotherm decreases rapidly. The Freundlich isotherm typically decreases rapidly with increased temperature and finally become almost single-valued at or above the boiling point of the adsorbed substance as adsorption capacity is greatly reduced. These characteristics of the Freundlich adsorption isotherm are very useful for understanding an adsorbed substance such as Hg, which has a low boiling point of 356.7°C. It means the adsorbed Hg can be desorbed easily and the different species will desorb at different temperatures (Sun et al., 2017). This is the foundation for a clean separation process that separates the adsorbed Hg in the form of a concentrated vapour phase that is easily removed from the solid adsorbent phase. Thermal desorption of Hg at temperatures above the boiling point of Hg should theoretically increase the rate of desorption by approximately as much as the difference between the vapour

pressure of Hg at high temperatures and the Hg-vapour pressure of the adsorbed Hg. Since the vapour pressure of the adsorbed Hg is near 10^{-5} atm at room temperature, it is possible to increase the desorption rate by as much as 10^{-5} atm by heating the adsorbent. This explains why reduction of the pressure using a vacuum has a much smaller effect on the desorption rate than temperature changes.

2.6.2 Adsorption using carbonaceous materials

Adsorption has been recognized as one of the most widely used method for removal of pollutant species from gaseous, aqueous solutions and ultimately from industrial effluents. Most adsorbents are derived from carbonaceous materials for the removal of variety of species from effluents (Bamdad et al., 2018; Carmalin and Lima, 2018; Crini et al., 2019). This is so because carbonaceous materials have high surface area, a microporous structure, and a high degree of surface reactivity which promote adsorption processes. Carbon used for adsorption is usually treated (activated) to make it very porous. There are various processing steps that can be followed to prepare carbonaceous materials into activated carbon for adsorption usage and each method has its disadvantages and advantages (Pietrzak et al., 2014). It is therefore pertinent to carry out optimisation studies when an adsorbent is being considered for commercial adoption for the first time. In this case, the best processing method will be selected based on adsorbent performance, cost and availability of requirements. Activated carbon has a large surface area that can adsorb relatively large volumes of materials per unity weight of carbon. There are two types of activated carbons, the powdered activated carbon (PAC) and the granulated activated powder (GAC) and these are used differently in the industry to remove contaminants from materials of interest. The PAC is added into the materials to adsorb pollutant substances while the GAC is packed into vessels that forms a filter bed/column (Stoquart et al., 2014).

2.6.3 Mercury adsorbents considered in this study

The disposal of used tyres poses significant challenges in modern society. Rubbers which are the main component of tyres are chemically among the most difficult materials to recycle because they are difficult to dissolve or melt. Tyres are a complex mixture of numerous different materials which include several rubbers, carbon black, steel cord and other organic and inorganic components. Different alternatives have been employed for tyre recycling such as re-use and

energy recycling. However, none of these approaches could eliminate the waste tyres disposal problem or could be economically exploited. Among the many waste tyre management options available, pyrolysis with its high energy recovering capability promises to be an environmentally acceptable method. The pyrolysis process is the thermal decomposition of organic wastes at high temperatures in an oxygen free environment. The process produces three different fractions in the following proportions: a solid fraction pyrolytic carbon black – (33 -38%), pyrolytic oil (38 – 55%) and a gas fraction (10 -30%) (Williams, 2013).

Several researches have been conducted on the characterization of tyres pyrolytic carbon black and some of these parameters infer good adsorption potential. Pyrolytic carbon parameters are reported in Table 2.1 with those of the well-known commercial carbon that has been previously used in various adsorption applications including Hg vapours adsorption. Despite pyrolytic carbon exhibiting these adsorptive properties, no studies have been directed towards its use in Hg adsorption where this useless byproduct can potentially find good application. The current study shall focus on the use of pyrolytic carbon as an alternative adsorbent for Hg vapours arising from fluorescent lamp waste recycling. Carbon black is a para-crystalline carbon that has a high surface-area–to–volume ratio. It is produced by the incomplete combustion process of heavy petroleum products such as tar, coal tar, ethylene cracking tar. Carbon black has a high surface area–to–volume ratio but lower than that of activated carbon. Pilusa and Muzenda (2013) describe the carbon black as a very fluffy fine powder with a large surface area which is composed essentially of elemental carbon. Carbon black is one of the most stable chemical products. Carbon black is generally and the most widely used nanomaterial and its aggregate dimension ranges from tens to a few hundred nanometres. Carbon black can be broadly defined as very fine elemental particles of carbon having a graphite-like bulk structure. Electron scanning, and XRD analysis methods have produced excellent results in the characterisation of carbon black surface microstructure.

Elemental composition of carbon black surfaces is different from its bulk content and the presence of some elements, especially, oxygen, is much richer on the surface. The oxygen atoms form different surface groups that play a significant role in the carbon black properties and its functionality (Song et al., 2020). The surface oxygen groups (hydroxyl groups) of the carbon black are collectively referred to as volatile content. The affinity of carbon black with materials, (e.g. paint, inks) is dependent on the type and amount of the functional groups on the surface.

Over 40 grades of carbon black are used for tyre manufacturing and many additional grades are marketed and used for manufacture of non-rubber related products. In South Africa, the major international tyre manufacturers account for more than over 80% of the carbon black consumption. Pyrolysis carbon black is produced as a solid by-product of waste tyre pyrolysis process after the gaseous fraction have been recovered and condensed into liquid fuels (Pilusa and Muzenda, 2013). Traditionally carbon black has been used as a reinforcement agent in tyre manufacturing. Because of its unique properties, today its uses have expanded to include conductive packaging in the Plastic industry and electrostatic discharge compounds, in the printing industry for toners and ink manufacturing and in material recovery as a potential absorber such as gold recovery and water purification. Activated carbon is a solid, porous, carbonaceous material prepared by carbonizing and activating organic substances (Shang et al., 2015).

Table 2.1: Comparative adsorption parameters of carbon black and commercial activated carbon

Property	Pyrolytic carbon	Activated carbon	References
Carbon content (%)	94	88.7	(Daniel et al., 2019; Djilani et al., 2015)
Sulphur content (%)	0.98	0.48	(Djilani et al., 2015; Wang et al., 2019)
Mesoporous ratio	68.27	76.3	(Lu et al., 2014; Wang et al., 2019)
BET Surface area (m^2/g)	121.47	797	(Lu et al., 2014; Wang et al., 2019)

Activated carbon is produced when any carbonaceous matter is carbonized and activated at high temperature with or without the addition of inorganic salts in a stream of activating gases such as steam or carbon dioxide. Alternatively, carbonaceous matter may be treated with a chemical activating agent such as phosphoric acid or zinc chloride and the mixture carbonized at an elevated temperature, followed by removal of the chemical activating agent by water washing. This research study shall use 30% hydrogen peroxide (H_2O_2) (Adelodun et al., 2014) and concentrated sulphuric acid (H_2SO_4) (Jawad et al., 2016) activated carbon black to adsorb and recover Hg from compact fluorescent lamp bulbs and compare its efficiency against the established and current commercial methods of Hg recovery from fluorescent lamps in South Africa.

2.6.4 Adsorption of gases and liquids

The phenomenon of adsorption normally occurs between solids and gases but is also known to take place between liquid-gas, liquid-liquid and solid-liquid systems (Coasne and Farrusseng, 2019; Monteillet et al., 2014).When a gas and a solid interact, intermolecular attractive forces will develop between them. If these intermolecular attractive forces are greater than those existing between molecules of gas itself, gas accumulates on the surface of solid. This phenomenon is called adsorption of gas on solid (Ponec et al., 2018). Adsorption is commonly confused with the term absorption. In absorption, a fluid (gas or liquid) permeates into or is dissolved by liquid or solid. Conversely, adsorption occurs only on the surface. Hence, adsorption is a surface phenomenon. The molecules adsorbed on the surface of solid are defined as "adsorbate" and the solid material upon which the adsorbate is adsorbed is defined as "adsorbent". Solid-gas adsorption is a surface process that leads to the transfer of gas molecules from fluid bulk to solid surface. Intermolecular forces lead to adsorption. Adsorption occurs in two ways, physical adsorption and chemical adsorption (Tran et al., 2017). Physical adsorption can also be referred to as physisorption. In physical adsorption, intermolecular forces causing adsorption between adsorbate and adsorbent are due to Van der Waals forces. Hence, physical adsorption is also referred to as Van der Waal's adsorption (Tao and Rappe, 2014). Physical adsorption is reversible due to weak forces. By heating or decreasing pressure, it can be reversed easily. The reverse of adsorption is defined as desorption. Physical adsorption is an exothermic process and heat is always released when adsorption occurs in order to form new bonds (Nguyen et al., 2016). Van der Waals forces causing adsorption are due to dipole-dipole, dipole-induced, London forces and possible hydrogen bonding. These forces are relatively weak compared to chemical forces; hence adsorption is a reversible process. In physical adsorption, the polarities of adsorbate and adsorbent play a very important role. Molecules can be polar or non-polar in characteristics. Polar molecules have a separate positive and negative charge which is called permanent dipole. In contrast to polar substances, positive and negative charges of nonpolar substances are in one centre, which means they have no permanent dipole. Moreover, most organic compounds are nonpolar due to their symmetry. Orientation, dispersion, or induction may cause physical adsorption. Positive polar adsorbent molecules and negative polar molecules of the adsorbate attract each other because of the orientation effect. In dispersion effect, a nonpolar adsorbate molecule is adsorbed by a nonpolar adsorbent. Nonpolar molecules do have

fluctuating dipoles due to the momentary changes in electron distribution round the atomic nuclei, which causes physical adsorption by dispersion effect (Christian et al., 2017; Tonigold and Groß, 2010).

2.7 Fluorescent Lamp Recycling and Mercury Recovery in South Africa

In South Africa Hg is released into the atmosphere from anthropogenic activities that include fossil-fuelled power plants, metal manufacturing industries, electrical and electronics manufacturing industries, cement plants, etc. There have always been wide discrepancies among researchers in estimations of mercury released into the atmosphere by South African industries (Gichuki and Mason, 2013). However, there is consensus among stakeholders that end-of-life CFLs result in Hg emissions hence their disposal must be carefully managed and incorporate a Hg recovery component. The major players in the recycling and disposal industry of the CFL lamp waste in South Africa include Reclite and E-Waste Africa. This study shall focus on the lamp recycling activities at Reclite plant facility in Germiston, South Africa. Generally, there is lack of clearly defined controls for CFL lamp waste recycling processes and technology amongst the current operators. The current processes and technologies implemented by the recyclers are not uniform but almost all include manual dismantling and mechanised shredding. The regulatory support of the technical role players in the waste recycling and recovery industry is also inadequate. The pieces of waste management regulations in place do not directly support or direct government financial resources towards the cause of recycling and recovery of hazardous waste (Ghosh et al., 2016). It is hard is generally hard to define how much CFL lamp waste is put on the market and how much ultimately becomes landfill waste. The industry is very heterogeneous and involves many stakeholders. Traditionally, CFL lamp waste has been a complex waste stream to manage in South Africa. The environmental sustainability of the adoption of this new energy efficient Hg laden compact fluorescent lighting technology in South Africa therefore needs to be investigated.

Traditional waste disposal methods such as land filling and incineration do not adequately address the aspects of Hg volatility which causes its escape into the atmosphere. These vapours subsequently settle and bioaccumulate in both the aquatic and terrestrial organisms. The crushing of fluorescent lamps into smaller components is the commonly the first step in the attempt to recover Hg. Other organisations alternatively remove the Hg containing phosphor powder by

using air vortex or by flashing with either sulphuric or hydrochloric acid (Wu et al., 2014). For the crushing option, the Drum-Top-Crusher technology (DTC), is one such method employed, and it reduces the volume of the waste which lessen the storage and handling costs associated with the fluorescent lamp waste management. The Drum-Top-Crusher consists of a vacuum-sealed container – a 55-gallon (210 litre) steel drum – in which glass fragments collect after passing through an entry tube and crushing mechanism as depicted in Fig 2.2. The Hg in the lamp waste is siphoned by the vacuum and gets trapped in a filter arrangement, which must be replaced periodically. Spent fluorescent lamps are typically hand-fed into the entry tube, rapidly drawn into the drum by the vacuum seal and crushed in the motorized crushing assembly. Once the storage container is full, it is replaced and shipped to a recycling facility for processing. Since the emergency and use of the DTCs, their efficiency in Hg vapour containment during the operation has been questioned and this led to several investigation studies conducted by different organisations, individuals and intuitions (Wilson et al., 2018).

Fig 2.2: Picture of a Drum Top Lamp Crusher. *Source* : (Schröder, 2017)

End-of-life CFLs are separated into their components while reclaiming (Hg) through established commercial technologies at Reclite a waste management company that recycles, treat and beneficiates electronic waste, notably, compact fluorescent lamp waste. The company utilises the state-of-the-art technology obtained from Sweden to achieve the high standard of operational compliance for the recovery of the hazardous Hg from the compact fluorescent lamp waste.

The Reclite factory produces the following as the by-products: Hg, phosphor powder, crushed glass, nonferrous metals, ferrous metals; plastic (various grades) and electronic components by following these processing steps which are depicted in Fig 2.3.

- The compact fluorescent tubes from different waste generators are fed into the machine where they are crushed into pieces.
- During the process, separation of materials according to density, particle size and conductivity takes place (i.e. metals and glass particles are separated).
- All the powder is transferred to cyclone dust and carbon filters from which the phosphor powder is collected in the barrel beneath the cyclone and sent to the distillation sections.
- The Hg laden air is forced through the activated carbon filters (ACFs) due to the negative pressure (vacuum) maintained in the filter units.
- As the air is forced through the activated carbon filters, the Hg is adsorbed onto the carbon and clean filtered air is released/vented into the atmosphere.
- The captured/adsorbed Hg in the activated carbon filters is later released and collected by thermo-treatment (retort).

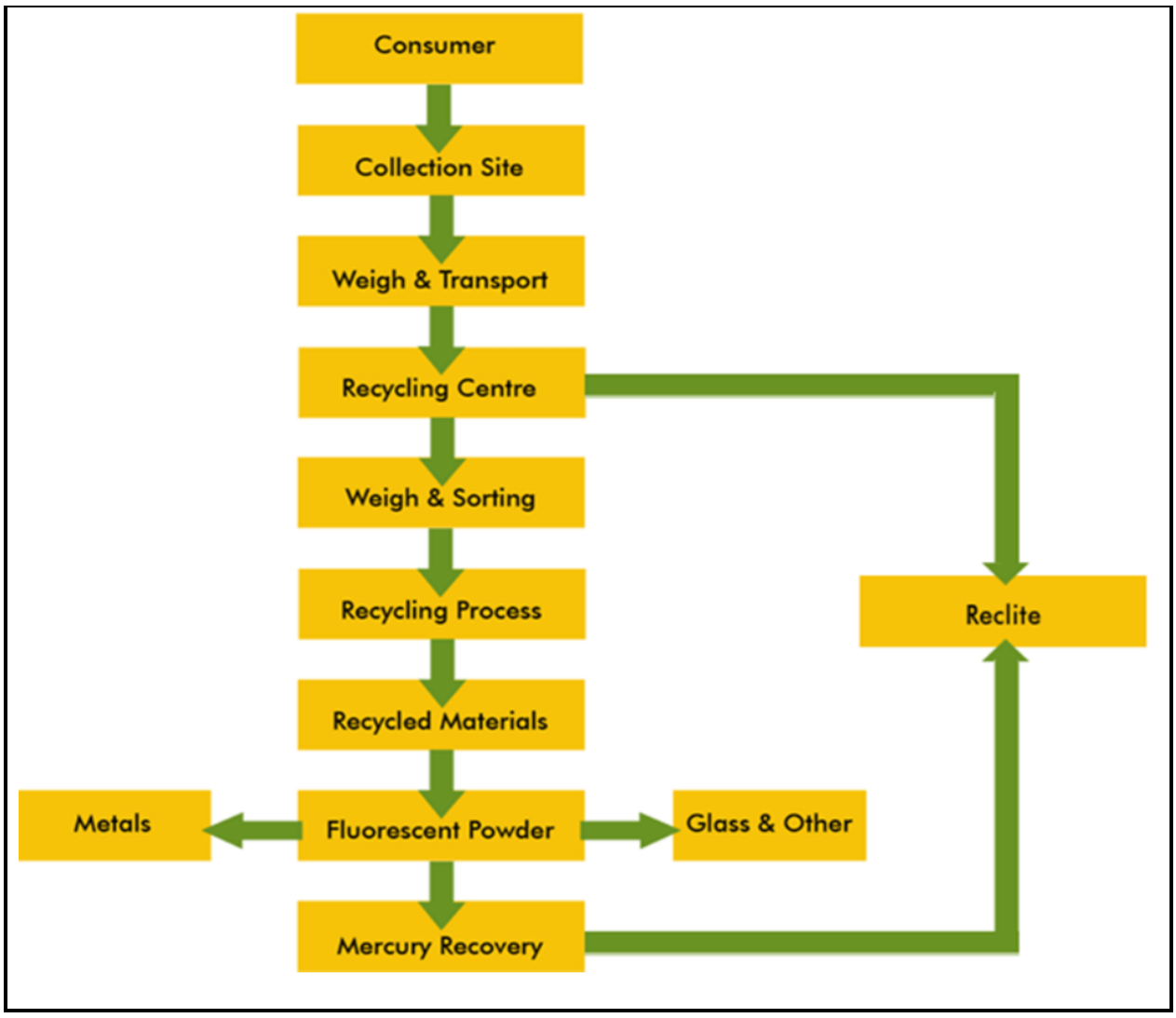

Fig 2.3: Reclite process flowsheet. *Source:* (Reclite, 2019)

2.8 Analytical Techniques

2.8.1 Principles of scanning electronic microscopy (SEM)

In the SEM unit electrons are generated by heating of the electron gun, which acts like a cathode. These electrons are propelled towards the anode, in the same direction as the sample, due to a strong electric field. After the beam of electrons is condensed, it enters the objective lens, which is calibrated by the user to a fixed position on the sample. Once the electrons strike the conductive sample, two things happen. First, the primary electrons that hit the sample will tunnel through it to a depth which dependant on the energy level of those electrons. Then, the secondary and backscattered electrons will hit the sample and reflect outwards from it. These reflected

electrons are then measured either by the secondary electron (SE) or backscattered (BS) detector. After signal processing takes place, an image of the sample is formed on the screen. In S Mode, secondary electrons are attracted by positive bias on the front of detector because of their low energy. The signal intensity is varied depending on the angle of the sample. Therefore, SE mode provides highly topographical images. On the other hand, in BS mode, the directions intensity is proportional to the number of the sample.

2.8.2 Principles of BBrunauer–Emmett–teller (BET)

The method is based on the principle that specific surface area of a powder is determined by physical adsorption of a gas on the surface of the solid and by calculating the amount of adsorbate gas corresponding to a monomolecular layer on the surface. Physical adsorption results from relatively weak forces (van der Waals forces) between the adsorbate gas molecules and the adsorbent surface area of the test powder are used to quantify the sample surface area. The determination is usually carried out at the temperature of liquid nitrogen. The amount of gas adsorbed can be measured by a volumetric or continuous flow procedure.

Single point measurement in BET

Normally, at least 3 measurements of V_a each at different pressure values of P/Po are required for the determination of specific surface area by the dynamic flow gas adsorption technique (Method I) or by volumetric gas adsorption (Method II). However, under certain circumstances described below, it may be acceptable to determine the specific surface area of a powder from a single value of Va measured at a single value of P/Po such as 0.300 (corresponding to 0.300 mole of nitrogen or 0.001038 mole fraction of krypton), using the following equation for calculating Vm:

$$S = \frac{V_m N_a}{m \times 22400} \qquad (2)$$

Where:

P = partial vapour pressure of adsorbate gas in equilibrium with the surface at 77.4 K (b.p. of liquid nitrogen), in pascals,

P_o = saturated pressure of adsorbate gas, in pascals,

V_a = volume of gas adsorbed at standard temperature and pressure (STP) [273.15 K and atmospheric pressure (1.013×10^5 Pa)], in millilitres,

V_m = volume of gas adsorbed at STP to produce an apparent monolayer on the sample

surface, in millilitres,

C = dimensionless constant that is related to the enthalpy of adsorption of the adsorbate gas on the powder sample.

N = Avogadro constant (6.022×10^{23} mol^{-1}),

A = effective cross-sectional area of one adsorbate molecule, in square metres (0.162 nm^2 for nitrogen and 0.195 nm^2 for krypton),

M = mass of test powder, in grams,

22400 = volume occupied by 1 mole of the adsorbate gas at STP allowing for minor departures from the ideal, in millilitres.

The specific surface area is then calculated from the value of V_m by equation (3) given above. The single-point method may be employed directly for a series of powder samples of a given material for which the material constant C is much greater than unity. These circumstances may be verified by comparing values of specific surface area determined by the single-point method with that determined by the multiple-point method for the series of powder samples. Close similarity between the single-point values and multiple-point values suggests that 1/C approaches zero. The single-point method can also be employed indirectly for a series of very similar powder samples of a given material for which the material constant C is not infinite but may be assumed to be invariant. Under these circumstances, the error associated with the single-point method can be reduced or eliminated by using the multi-point method to evaluate C for one of the samples of the series from the BET plot. Here, C is calculated as (1 + slope/intercept). Then V_m is calculated from the single value of V_a measured at a single value of P/P_o by the equation:

$$V_m = V_a\left(1 - \frac{P}{P_o}\right) \qquad (3)$$

The specific surface area is calculated from V_m by equation (3) given above (Particle Analytical, 2019).

Surface area measurement by BET

This method for determining the surface area of a porous solid was developed by Brunauer, Emmett, and Teller and is a widely used tool for determining the monolayer volume (Vm) and the specific surface area (As). The BET method is based on gas sorption (both adsorption and desorption) on the surface of dry solid powders. Nitrogen, N_2, adsorption at 77 K and at sub-

atmospheric pressures represents the most widely used technique to determine catalyst surface area and to characterize its porous texture. Nitrogen is applied over a wide range of relative pressures ($p = p_o$) and produces adsorption isotherms that provide information on size distributions in the micro-, meso- and macroporosity ranges approximately 0.5–200 nm. The amounts of gas molecules adsorbed or desorbed are determined by the pressure variations due to the adsorption or desorption of the gas molecules by the material (the adsorbent). The total surface area of the adsorbent is calculated using the adsorption model and the total area that will be occupied by the nitrogen. The surface area, S equation 4 is given below:

$$S_{BET} = V_m N_a \sigma_x / V \qquad (4)$$

Measurement of pore size distribution using BET

Pore size distribution (PSD), a very important property of adsorbents, determines the fraction of the total pore volume accessible to molecules of a given size and shape. Pores can have a regular and/or irregular shape. In most cases these pores are of different sizes. According to the IUPAC definitions the pore sizes of activated carbon can roughly be classified as micropores (< 2 nm), mesopores (2 - 50 nm) and macropores (> 50 nm). The macropores act as transport pathways, through which the adsorptive molecules travel to the mesopores, from where they finally enter the micropores. Thus, macro- and mesopores can generally be regarded as the highways into the zeolite particle and are crucial for kinetics. The micropores usually constitute the largest proportion of the internal surface of the zeolite and contribute most to the total pore volume.

2.8.3 Principles of X– ray diffraction

The X – Ray Diffraction analysis is based on constructive interference of monochromatic X-rays and a crystalline sample: The X-rays are generated by a cathode ray tube, filtered to produce monochromatic radiation, collimated to concentrate, and directed toward the sample. The interaction of the incident rays with the sample produces constructive interference (and a diffracted ray) when conditions satisfy Bragg's Law ($n\lambda=2d \sin \theta$). This law relates the wavelength of electromagnetic radiation to the diffraction angle and the lattice spacing in a crystalline sample. The characteristic x-ray diffraction pattern generated in a typical XRD analysis provides a unique "fingerprint" of the crystals present in the sample. When properly interpreted, by comparison with standard reference patterns and measurements, this fingerprint allows identification of the crystalline form. X-Ray Diffraction analysis assist with the

measurement of the average spacing between layers or rows of atoms in a sample, determine the orientation of a single crystal or grain, find the crystal structure of an unknown material and measure the size, shape and internal stress of small crystalline regions (Particle Analytical, 2019).

2.8.4 Principles of Fourier transform infrared (FTIR)

FTIR spectrometers (Fourier Transform Infrared Spectrometer) are widely used in organic synthesis, polymer science, petrochemical engineering, pharmaceutical industry and food analysis. In addition, since FTIR spectrometers can be hyphenated to chromatography, the mechanism of chemical reactions and the detection of unstable substances can be investigated with such instruments.

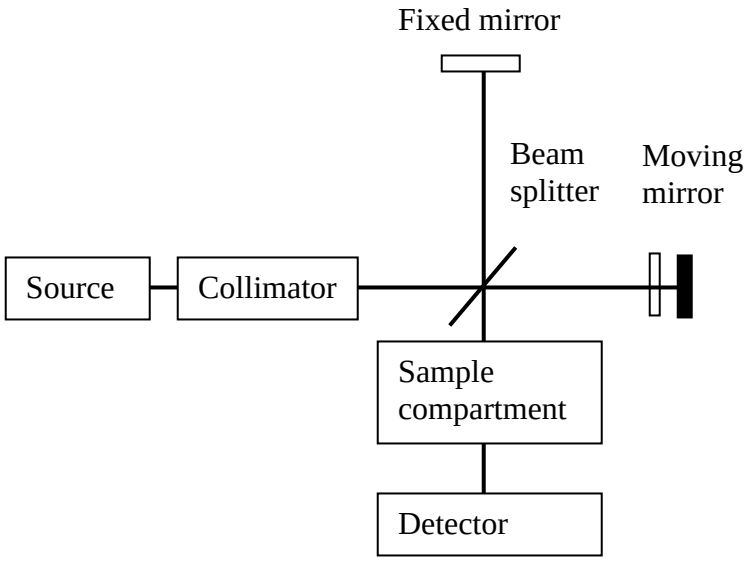

Fig 2.4: Block diagram of an FTIR spectrometer. *Source*: (Birkner and Wang, 2020)

A common FTIR spectrometer consists of a source, interferometer, sample compartment, detector, amplifier, A/D convertor, and a computer. The source generates radiation which passes the sample through the interferometer and reaches the detector. Then the signal is amplified and converted to digital signal by the amplifier and analog-to-digital converter, respectively. Eventually, the signal is transferred to a computer in which Fourier transform is carried out. Fig 2.4 is a block diagram of an FTIR spectrometer.

Fourier Transform of Interferogram to Spectrum

The interferogram is a function of time and the values outputted by this function of time are said to make up the time domain. The time domain is Fourier transformed to get a frequency domain, which is deconvolved to produce a spectrum. Fig 2.5 shows the Fast Fourier transform from an interferogram of polychromatic light to its spectrum.

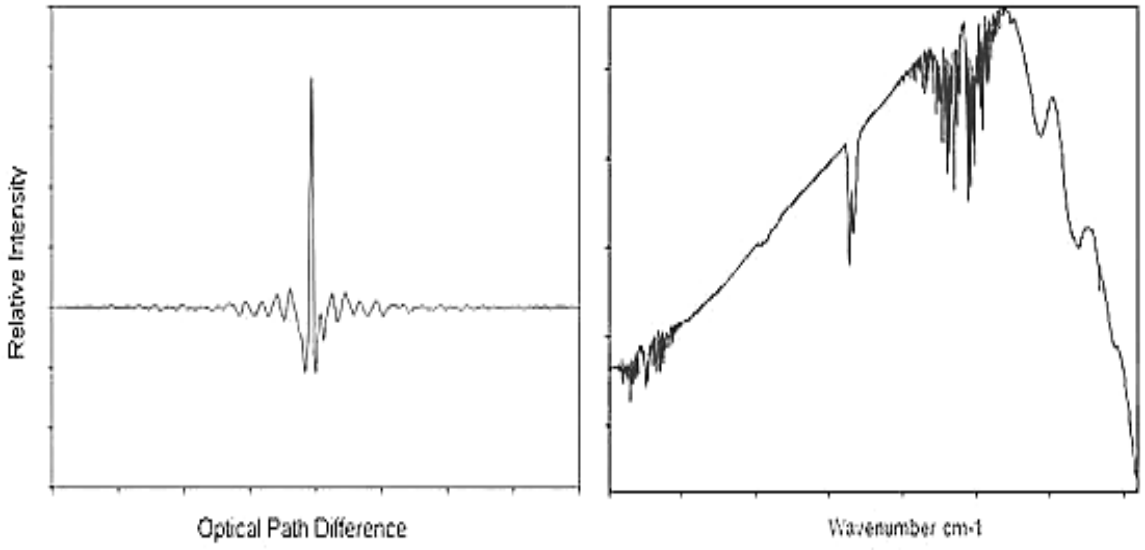

(a) (b)

Fig 2.5: (a) Monochromatic light interferogram and, (b) its spectrum.
Source: (Birkner and Wang, 2020)

Simplified Math Description of the Fourier Transform in FT-IR

The wave functions of the reflected and transmitted beams may be represented by the general form of:

$$E1 = rtcEm \times \cos(vt - 2\pi kx)(7)(7)E1 = rtcEm \times \cos(vt - 2\pi kx) \quad (5)$$

and

$$E1 = rtcEm\cos[vt2\pi kx(vx + \Delta d)](8)(8)E1rtcEm \times \cos[vt - 2\pi k(vx + \Delta d)] \quad (6)$$

Where

- Δd is the path difference,
- r is reflectance (amplitude) of the beam splitter,

- t is the transmittance, and
- c is the polarization constant.

The resultant wave function of their superposition at the detector is represented as:

$$E = E1 + E2 = 2(r \times t \times c \times Em) \times \cos(vt - 2\pi kx)\cos(\pi k\Delta d)(9)(9)E = E1 + E2 = 2(r \times t \times c \times Em) \times \cos(vt - 2\pi kx)\cos(\pi k\Delta d)$$

(7)

Where $E_{m,}$ ν, and k are the amplitude, frequency and wave number of the IR radiation source.

The intensity (I) detected is the time average of E_2 and is written as

$$I = 4r2t2c2E2m\cos 2(vt - 2\pi kx)\cos 2\pi k\Delta d)(10)(10)I = 4r2t2c2Em2\cos 2(vt - 2\pi kx)\cos 2(\pi k\Delta d)$$

(8)

Since the time average of the first cosine term is just ½, then

$$I = 2I(k)\cos 2(\pi k\Delta d)((11)(11)I = 2I(k)\cos 2(\pi k\Delta d) \quad (9)$$

And

$$I(\Delta d) = I(k)[1 + \cos(2\pi k\Delta d)]((12)(12)I(\Delta d) = I(k)[1 + \cos(2\pi k\Delta d)] \quad (10)$$

where I(k) is a constant that depends only upon k and I(Δd) is the interferogram.

From I(Δd) we can get I(k) using Fourier transform as follows:

$$I(\Delta d) - (\infty) = \int km01(k)\cos(2IIk\Delta d)dk(13)(13)I(\Delta d)(-I(\infty) = \int 0kmI(k)\cos(2IIk\Delta d)dk$$

(11)

Letting $K_m \rightarrow \infty$, we can write

$$I(k) = \infty 0[(\Delta d) - I(\infty)]cos\ 2(IIld\Delta d(14)(14)I(k) = \int 0\infty[I(\Delta d) - I(\infty)]\ cos\ 2IIk\Delta d)(d\Delta d$$

(12)

The physically measured information recorded at the detector produces an interferogram, which provides information about a response change over time within the mirror scan distance. Therefore, the interferogram obtained at the detector is a time domain spectrum. This procedure involves sampling each position, which can take a long time if the signal is small and the number of frequencies being sampled is large.

In terms of ordinary frequency, νν, the Fourier transform of this is given by (angular frequency ω=sπνω=sπν):

$$f(v) = \int \infty - \infty f(t)e - i2IIvtdt(15)(15)f(v) = \int -\infty\infty f(t)e - i2IIvtdt \quad (13)$$

The inverse Fourier transform is given by:

$$f(v) = \int \infty - \infty f(t)e + i2IIvtdt(16)(16)f(v) = \int -\infty\infty f(t)e + i2IIvtdt \quad (14)$$

The interferogram is transformed into IR absorption spectrum (Fig 2.5 and Fig 2.6) that is commonly recognizable with absorption intensity or % transmittance plotted against the wavelength or wavenumber. The ratio of radiant power transmitted by the sample (I) relative to the radiant power of incident light on the sample (I_0) results in quantity of Transmittance, (T). Absorbance (A) is the logarithm to the base 10 of the reciprocal of the transmittance (T).

$$A = \log 10T = -\log 10II0(17)(17)A = \log 101T = -\log 10T = \log 10II0 \quad (16)$$

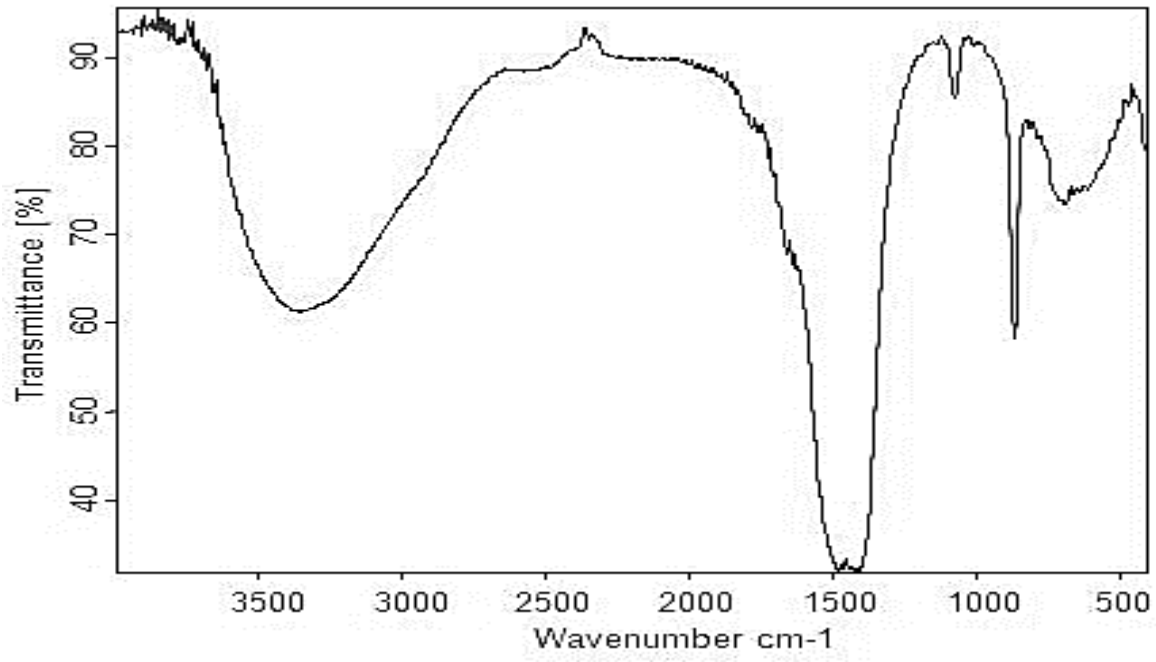

Fig 2.6: Infra-Red spectrum of a sample. *Source:* (Birkner and Wang, 2020)

To interpret the FTIR spectra of Fig 2.6 the band peaks observed above wave number 1500 cm^{-1} (4000 to 1500) represent group frequencies for small functional groups groups such as -COOH

(for organic acids), -OH (for alcohols or inorganic hydrocides), -CO (in ketones and aldehydes), etc. Bands below wavenumber 1500 cm^{-1} (1500 to 500) represent fingerprint frequencies which give a pointer to a full molecule or compound identification. However other functional groups can also give peaks in the fingerprint region. Therefore, sole reliance on information from this region is inappropriate for compound and functional groups identification. Peaks and corresponding compounds/functional groups are matched with the help of vast Infra-Red spectra library/databases available on the market.

2.9 Chapter Conclusions

Mercury is a volatile substance, that sublimes at room temperature and can easily be absorbed by living organic matter (plants and animals). The substances bioaccumulates as it goes up in the food chain. Hg has adverse health effects on human beings. Methylmercury is toxic to the central peripheral nervous systems, harmful to the digestive and immune systems as well as lungs and kidneys. It is because of this reason, that the substance Hg or containing Hg has been classified as hazardous. Besides the beneficial effects of Hg in the new fluorescent lighting technology, the above mentioned environmental and health effects remain the greatest challenge in the use and disposal of compact fluorescent lighting lamp waste. From the literature reviewed, it has been established that most of the technologies on control and recovery of Hg from fluorescent lamps emerged from the developed nations. However, much research still needs to be done on cheaper and locally available technological solutions or retrofits to these imported technologies to reduce costs of adopting these technologies in Africa. Numerous research studies highlighted the challenge of direct release of Hg vapour from used, broken and end of life fluorescent lamp products in a developing African state. This study attempts to develop and provide an alternative safe and sustainable technology in the recovery of Hg vapour during the recycling and processing of the compact fluorescent lamp waste in South Africa.

CHAPTER THREE: RESEARCH METHODOLOGY

3.0 Chapter Overview

This chapter discusses the different research methods and tools that were used in conducting this research. The laboratory experiments and activities that shaped this research are documented. These experiments were dictated by the project objectives. The main objectives for carrying out this research included producing activated carbon from the pyrolytic residues of waste tyres. This would be followed by testing if that carbonaceous product could be used as an adsorbent for Hg vapours during fluorescent lamp recycling. The properties of the tyre pyrolytic carbon-based adsorbent were compared against those of commercially available and currently used activated carbon. The additional objective was to evaluate which of the two carbon activation processes, sulphuric acid or hydrogen peroxide would produce a better adsorbent for mercury removal. The activation procedures, experimental set up for adsorption trials and the analytical techniques employed are all described under this section.

3.1 Experimental Design

A number of experimental activities were performed in a sequential pattern. The workflow activities are depicted in Fig 3.1 and briefly described here. Detailed explanation for each activity is given in the next sections. Firstly, raw pyrolytic carbon was sourced from a tyre pyrolysis factory. This carbon went through different preparation stages so that it could be characterised, activated and used for adsorption trials. Two activation procedures one involving sulphuric acid and the other involving hydrogen peroxide were followed. After activation the two differently activated carbons were used in adsorption trials. The adsorptive properties of these two carbons were compared to those of saturated commercially available carbon that is currently being used at a local mercury waste recycling plant (Reclite) in South Africa.

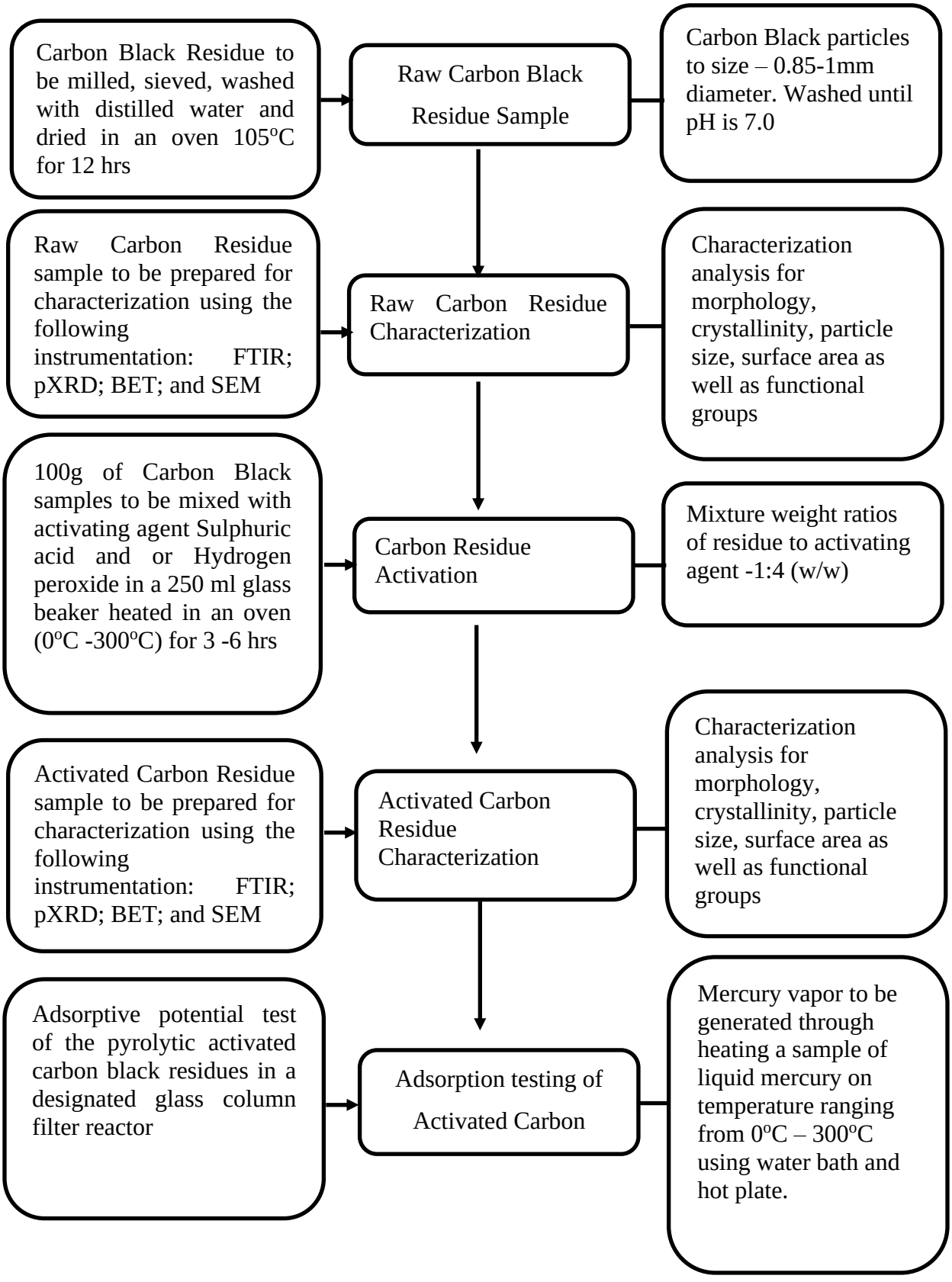

Fig 3.1: Flow diagram of the experimental activities performed

3.2 Experimental Materials

3.2.1 Chemical reagents and glassware

Chemicals and reagents that included 99% sulphuric acid (H_2SO_4), 32% hydrochloric acid (HCl), 30% hydrogen peroxide (H_2O_2), de-ionised water, etc were obtained from Sigma-Aldrich Merck (South Africa). These chemicals were all analytical grade and were used as received unless stated otherwise. Glassware were obtained from Glass world.

3.2.2 Adsorbents

The pyrolytic carbon black residue was obtained from the pyrolysis of waste tyres process of RECO, a company based in Pretoria (South Africa). The residue appeared black with a granulated fluffy texture. According to certificates of analysis from the company's Quality Control department, the raw pyrolytic carbon black contained 95% w/w carbon 2% w/w sulphur and the rest were inorganics. The granular pyrolytic carbon black sample from RECO was in irregular fluffy form with evident ash content. Saturated activated carbon was obtained from Reclite, a fluorescent lighting recycling company in South Africa. They are currently recovering mercury vapours from their process using a commercially available activated carbon as adsorbent (See section 2.7 in this report). The saturated activated carbon sample is a product of this adsorption process and it is pictured in Fig 3.2.

Fig 3.2: Picture of saturated commercial grade activated carbon sample from Reclite.

3.2.3 Laboratory equipment

Analytical equipment used for characterisation are those from the Chemistry department at the University of Witwatersrand housed within the Chemistry laboratory. Some of these equipment included for FT-IR the Perkin Elmer System 2000 FT-IR, for SEM/EDX the Jeol JSM-6390 LV SEM with Noran system Six software, for XRD the Diffractometer instrument - Bruker AXS D8 Advance and for BET a Micrometrics Accelerated and Porosimetry (ASAP) 2010 system with nitrogen used as probe gas was used. Also used were an electric Labotec oven with operating temperature range 0 – 1000^{o}C, a desiccator, vacuum filter, vacuum pumps, Mortar and pestle, Sieve size 0.85–0.1 mm, several glassware, etc. Photographs of the analytical equipment used are displayed in Figure 3.3

Fig 3.3: Analytical equipment used for (a) FTIR (b) XRD (c) BET (d) SEM/EDX

3.3 Methods Description

3.3.1 Carbon preparation

The raw pyrolytic waste tyre carbon black sample of 400g was first washed with hot water. The sample was then dried in a drying oven at a temperature of 120°C overnight. After cooling, the carbon black sample was then milled using a lab scale handheld mortar and pestle. Milled material was sieved and the undersized parties in the size class 0.85–0.1 mm diameter was collected and kept for further experimentation. Dry saturated commercial activated carbon was also pulverised. The milling equipment and products are depicted in Figure 3.4. The oversized material went through continued milling until the whole sample material was in the desired particle size class.

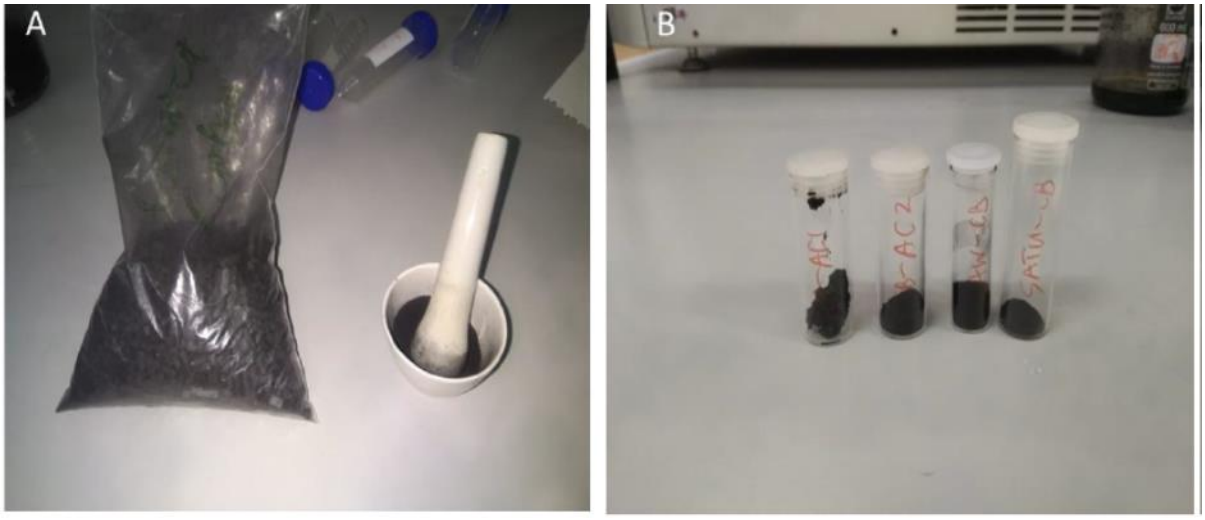

Fig 3.4: (A) Milling equipment (B) Milled carbon and commercial activated carbon

The resulting powdered carbon black was washed in 1M HCL and thereafter in hot distilled water until a pH 7.0 of was achieved. This sample of carbon black material was then dried in an oven at 105°C for 24 hours in preparation for activation. The carbon preparation steps described under this section are shown in Fig 3.5 and the prepared carbon is pictured in Fig 3.6.

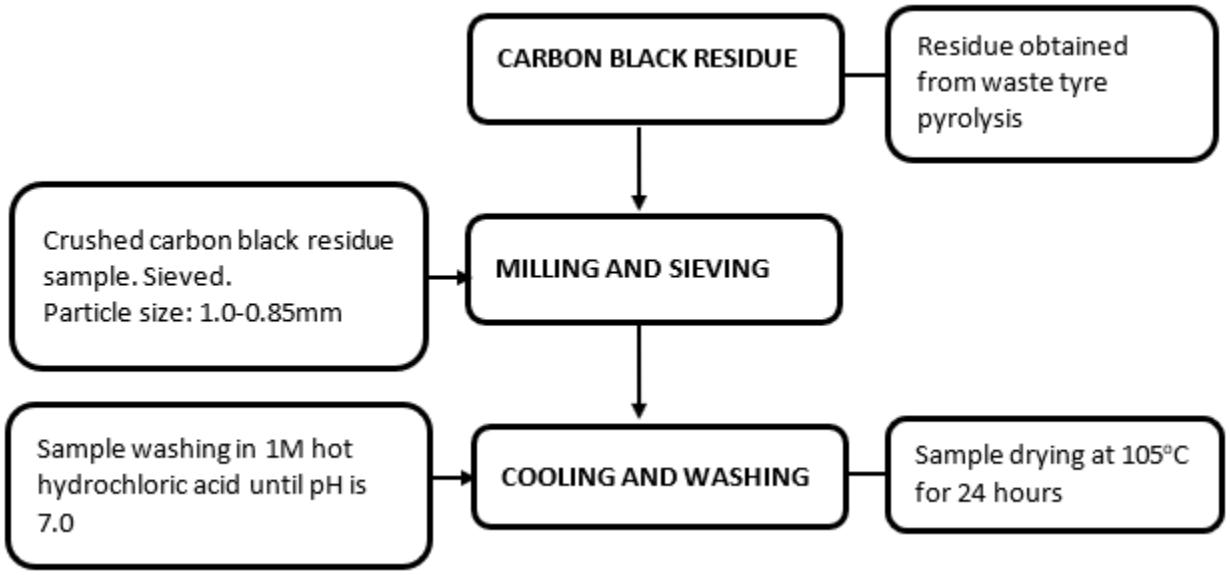

Fig 3.5: Flow diagram of ccarbon sample preparation

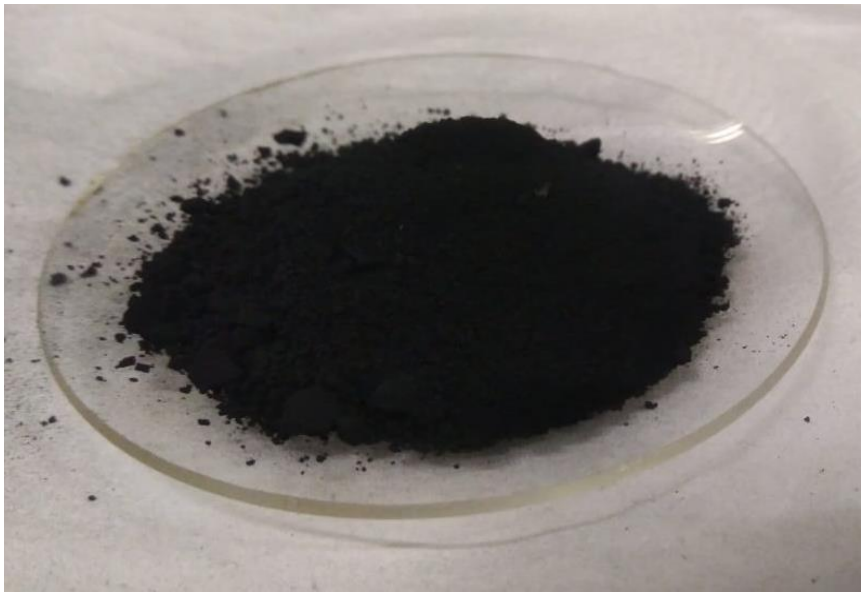

Fig 3.6: Picture of prepared carbon black sample residues

3.3.2 Adsorbent characterisation

The characterisation was applied to determine the qualitative and structural properties of the carbonaceous residue materials under consideration in this research study. The analytical methods employed have been chosen as the most suitable ones considering instrument and material availability as well as costs involved in analysis. The selected methods and techniques were adapted to enhance the accuracy and precision of analysis of the material as far as possible.

Analysis were performed before activation, after activation and after adsorption trials for the carbon black. The purpose of each type of technique is stated in Table 3.1. Briefly, the adsorbents were characterized using FTIR, SEM/EDX, BET and pXRD techniques.

Table 3.1: Adsorbent characterisation techniques and their purposes

Purpose	**Type of Technique**
Determine and reveal functional groups	Fourier Transform Infrared (FTIR)
Crystallinity, particle size, phase identification, pore diameter.	X-Ray Diffraction Analysis (XRD)
Identification of morphology (shape and size of particles) with EDX revealing the chemical composition of the sample, including what elements which will present as well as their distribution and concentration	Scanning Electron Microscope/Energy Dispersive X-ray (SEM/EDX)
Surface area and pore diameter, Porosity analysis	Brunauer-Emmet-Teller (BET)

Fourier Transform Infrared (FTIR)

The FTIR (Fourier Transform Infrared) analysis was performed to reveal the qualitative organic part of the pyrolytic carbon, both in the raw and the activated materials. The analysis was achieved by transmittance technique on the tablet of potassium bromide (KBr). The sample was placed in a Thermo Nicolet, spectrophotometer under laboratory and the instrument sweeps were set at 64 with a resolution of 4 cm^{-1} and a rate of 0.6329. The DGTS of KBr detector was used in the range of 400 – 4000 cm^{-1} (wave number). For the tablet development, 200 mg of KBr previously dried at 80^{o}C in an oven vacuum for 24hours, were weighed and mixed with small amount of the carbon powder. The mixture was placed in a tablet hole and a force of 9 tons was applied for 5 minutes in order to compact the tablet sample before testing (A. Azamar et al, 2008). Samples that went through FTIR analysis were labelled properly and these were the raw tyre waste carbon black (RAW-CB), saturated commercial carbon black (SATU-CB). Samples derived from later activation experiments involving carbon black activation by sulfuric acid CB-AC1) and hydrogen peroxide (CB-AC2) were also subjected to FTIR analysis.

Powder X-Ray Diffraction analysis

The pXRD (powder X-Ray Diffraction) analysis was carried out in order to characterise the adsorbent crystallinity, particle size, pore diameter and phase identification. Four samples were analysed by pXRD technique and these are the raw tyre waste carbon black (RAW-CB), saturated commercial carbon black (SATU-CB) then from later experiments, the sulfuric acid activated carbon black (CB-AC1) and the hydrogen peroxide activated carbon black (CB-AC2). The analysis was performed using a Diffractometer instrument - Bruker AXS D8 Advance. A sample of the adsorbent was milled to particle sizes in the range of 0.002- 0.005 mm cross section to have homogeneity and for the crystallites to be randomly distributed. The sample was then pressed into a sample holder to obtain a smooth flat surface. The Diffractometer was operated at 40V and 30A using a copper-filtered copper-K radiation with a wavelength of 1.541 Å. The diffraction pattern of the sample was obtained by scanning the sample in an interval angle of 2θ from 20 - 100° and at a rate of 2/0.02 (degrees).

The scanning electron microscope (SEM/EDX) procedure

This analysis was carried out to evaluate the adsorbent surface morphology from SEM while the EDX revealed the elemental composition of the adsorbents. The samples for SEM/EDX analysis were the raw tyre waste carbon black (RAW-CB) and the saturated commercial carbon black (SATU-CB). Samples of raw carbon black (RAW-CB), activated carbons (CB-AC1 and CB-AC2) before and after adsorption trials were analysed. Briefly, the sample was placed onto sample stub and the carbon tape was used to adhesively bond the sample to the stub. The sample was placed into a gold sputtering system and onto the SEM sample holder. The SEM Instrument was started up for analysis. This procedure was repeated for all the samples and results were downloaded from the instrument.

Brunauer–Emmet–Teller (BET) instrument procedures

The adsorbents' surface area, pore volume and pore size distribution were determined by means of the BET technique using a Micrometrics Accelerated and Porosimetry (ASAP) 2010 system and nitrogen as probe gas. Raw pyrolytic waste tyre carbon black (RAW-CB), saturated commercial carbon black (SATU-CB), sulfuric acid-based carbon black activated carbon (CB-AC1), and hydrogen peroxide-based carbon black activated carbon (CB-AC2) were also analysed with BET. Approximate sample of 20 mg was placed and sealed in a sample tube. The samples were degassed and dried at 165^{o}C under vacuum. Afterwards the sample was cooled

down and weighted again to determine possible mass loss. Now the sample holder was placed in the BET measurement unit then analysis started by sample cooling down to -196 ^{o}C. Cooling was followed by a constant nitrogen injection flow to determine the N_2 displacement for specific surface area calculation.

3.2.3 Adsorbents activation

Prior to use in adsorption studies, the adsorbents were activated to improve their adsorptive properties. A one-step chemical activation method was used to prepare activated carbon from the raw pyrolytic powder. The activation using this method proceeded in a drying oven that was connected to a fume hood as shown in Figure 3.7. Two chemical activating agents, sulphuric acid (H_2SO_4) and hydrogen peroxide (H_2O_2) were used in this study, in a 1:4 ratio (carbon black: activating agent) (Adelodun et al., 2014; Matandabuzo and Ajibade, 2018). The sequential process activities in volved in carbon activation are outlined in Figure 3.8 with some activating agent specific descriptions detailed in in the following paragraphs.

Activation of carbon black (CB) using sulphuric acid

Carbon activation using 99% H_2SO_4 was performed. Approximately 100 g of powdered and dried carbon black was impregnated with 100 mL of H_2SO_4 and the impregnation mixture was kept for 12 hours in an oven at 100 ºC as shown in Fig 3.7. The mixture was further heated in an oven for 6 hours at temperatures ranging from 200-280 °C as stated in Fig 3.8. A black bubbles-like structure of activated carbon was produced which was allowed to cool. Upon cooling, the activated carbon was rinsed with hot distilled water to remove acid from the activated carbon until the pH of the resulting solution was neutral, that is, pH = 7. The resultant activated carbon was further dried in an oven at 120 °C overnight. The final product is the one referred to as sulphuric acid-based carbon black-activated carbon (CB-AC1) in this report.

Fig 3.7: Carbon chemical activation in an electric oven

Activation of carbon black (CB) using hydrogen peroxide

In this study, for activation, 100 g of dried-sieved carbon black was impregnated with 100 mL of hydrogen peroxide (H_2O_2) and the impregnation mixture was kept for 12 hours in an oven at 100 ºC as demonstrated in Figure 3.6. The mixture was heated in the oven for 6 hours at temperatures ranging from 200-280 °C as portrayed in Figure 3.7. Activated carbon was produced and allowed to cool to room temperature. Upon cooling, the activated carbon was rinsed with cold distilled water to remove hydrogen peroxide from the activated carbon. The resultant activated carbon was further dried in an oven at 120 °C overnight. The resultant product was appropriately labelled as CB-AC2 then stored for later use.

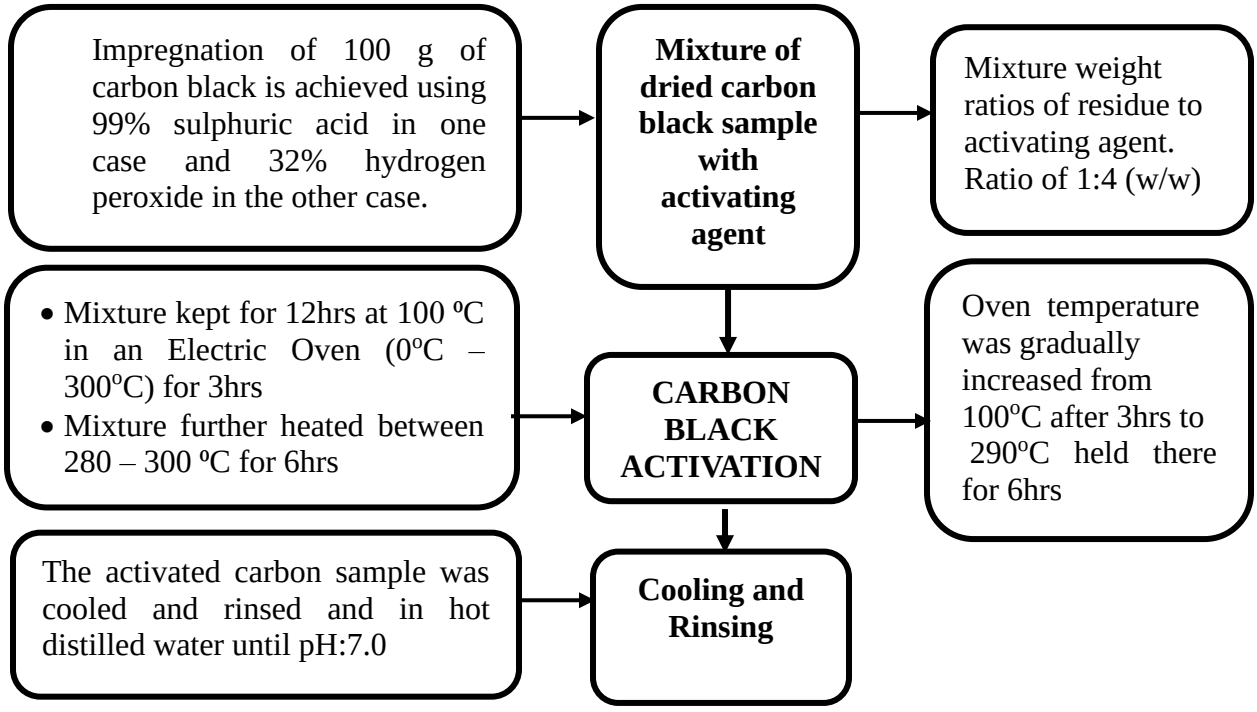

Fig 3.8 Cchemical activation processes for carbon black

3.3.4 Adsorption Trials

The determination of the Hg vapour adsorption of the prepared activated carbon was done through an experimental set up pictured in Fig 3.9. A sample of liquid Hg (4.89 mg) was put in a 250 mL flask. The flask was placed in a water bath whose water temperature was maintained at 100C^{o} under normal atmospheric pressure. This flask was connected to a glass column filter packed reactor. Activated carbon (0.055 g) samples had been previously loaded into this reactor. The reactor was connected to an active peristaltic air vacuum pump. This experimental set up under these conditions was allowed to run for 6 hours before stopping and analysing the adsorbents. The same experimental activities were repeated using an electric hotplate as the heat source at a temperature of 300ºC instead of the water bath. This experimental set up was run under an active laboratory fume hood cupboard to ensure safe extraction and emission of all potential fugitive Hg vapours. Refer to flow diagram Fig 3.10 for details described here.

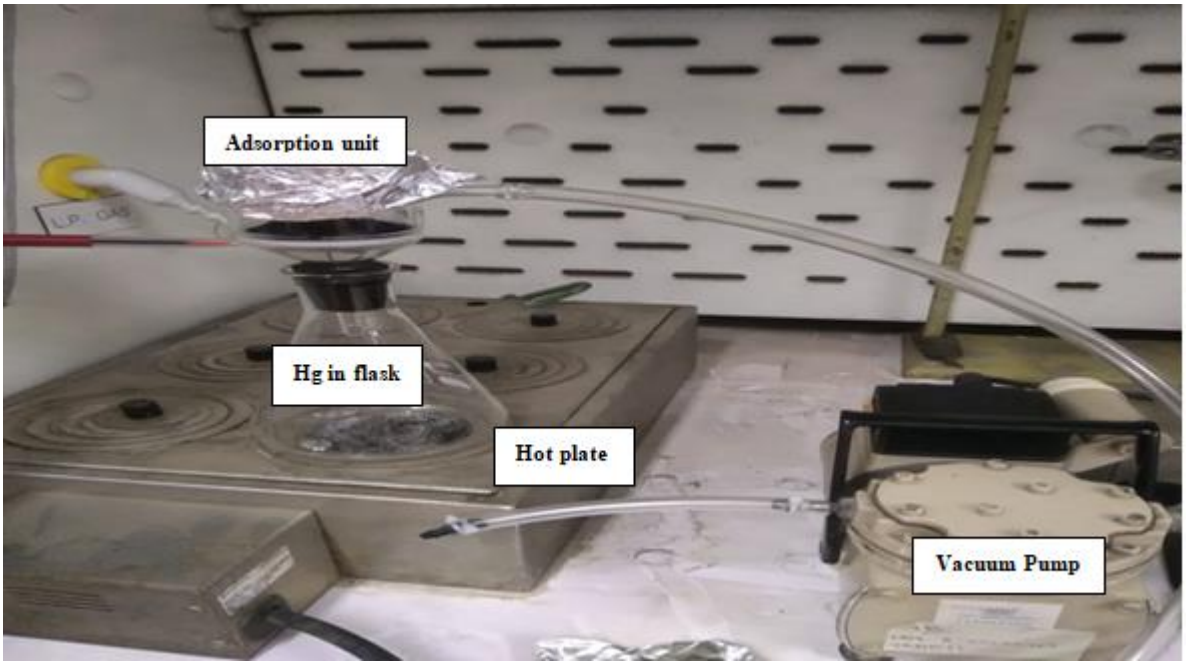

Fig 3.9**:** Mercury adsorbents testing set up.

(A peristaltic vacuum pump is connected to the filter unit to extract the Hg vapour under the fume wood cupboard)

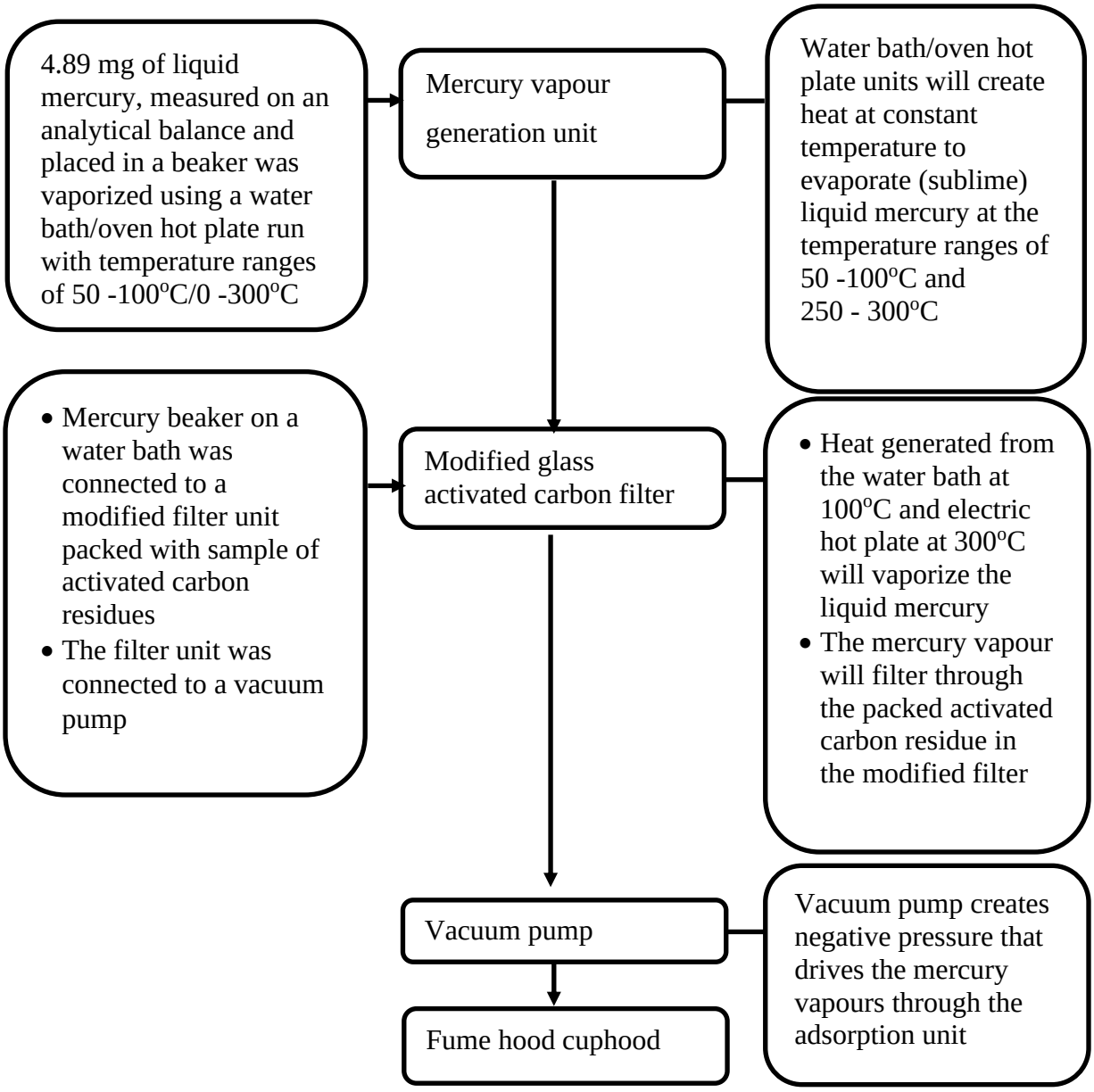

Fig 3.10: Flow diagram of Hg vapour adsorbents testing

3.5 Desorption process

The saturated commercially available carbon (SATU-CB) was subjected to a thermal desorption process by merely heating the adsorbent at a temperature of 600°C for 48 hours (Ho et al., 2005). Desorption was performed in similar set up as activation (Fig 3.7). Desorption restored the saturated carbon to its "before adsorption" status. In this status the pXRD, FTIR and BET analysis were then performed on the adsorbent. The SEM/EDX evaluations were done before the desorption process.

3.7 Chapter Conclusions

This chapter focussed mainly on the methods used in conducting this research project. These methods included the preparation and synthesis of activated carbon from waste tyres pyrolysis. The adsorption trials for the prepared activated carbon are also described. The adsorbent characterization techniques and conditions used are also outlined. Briefly the one-step carbon synthesis route was used. Activation was achieved for one sample by sulphuric acid activation and for the other sample by hydrogen peroxide activation. These choices of activation agent were based on sulphuric acid ($H_2SO_{4)\ being}$ a strong acid, strong oxidant and strong dehydrating agent. On the other hand, hydrogen peroxide (H_2O_2) is a weak acid, also strong oxidant, eco-friendly and efficient. These properties from both chemicals have since been proven to improve adsorbent surface properties towards better adsorption properties. Choosing two activating agents was done to compare if tyre pyrolytic carbon activation was amenable to variations in the agent used. The characterisation techniques used in this investigation include FTIR, BET pXRD and SEM/EDX spectrometry. The design of the adsorption reactor was more influenced by the study objective of ensuring a product that can be produced and perform sustainably hence the limit of the experimental temperatures to within 300 ^oC.

CHAPTER FOUR: RESULTS AND DISCUSSION

4.0 Chapter Overview

Results accrued from the methodologies outlined in chapter 3 are recorded in the current chapter and discussed thereafter. The discussions are taken in line with the study aim, research questions and the set objectives. Adsorption properties and performance by samples of the activated carbon developed with different activating agents were compared to the performance exhibited by commercially available activated carbon.

4.1 Results and Discussion of FTIR Analysis

The results of FTIR results of the carbon black, its activated carbons and that of commercial activated carbon are shown in Fig. 4.1. Absorption bands around 1100 cm^{-1} with an overtone at 1430 cm^{-1} shown in Fig 4.1(A) correspond to Si-O-Si asymmetric stretch (Makam et al., 2018). The C=C stretching vibration attributed to the lignocellulose aromatic structure appeared at 1657-2000 cm^{-1} in carbon black and in activated carbons (Heo and Park, 2018; Makam et al., 2018). Another vibration band at 2345 cm^{-1} appeared in both carbon black and activated carbons and this can be assigned to the alkyne groups. However, it was also observed that the IR spectrum of raw carbon black showed less functional groups as compared to the sulphuric acid and hydrogen peroxide-based activated carbons. The latter could be due to the fact that, during/after activation, various functional groups are formed. The C-O-C stretching vibrations in ether, phenol and esters groups appeared between 1041–1248 cm^{-1}. In their study, (Heo and Park, 2018) also reported acyclic C-O-C groups around 1300-1000 cm^{-1} coupled with aromatic structures (C=C). The stretching vibration band at 1000 cm^{-1} is attributed to C-O group and is distinct in sulphuric acid-based activated carbon. It has been reported that chemical activation with hydrogen peroxide oxidant normally yield carbonaceous structures with oxygen-functionalities on the surface (Heo and Park, 2018). These claims were also observed in this study, and these functionalities are known for participation in the activated carbon-Hg interaction which overally influences the Hg adsorption rate by activated carbons.

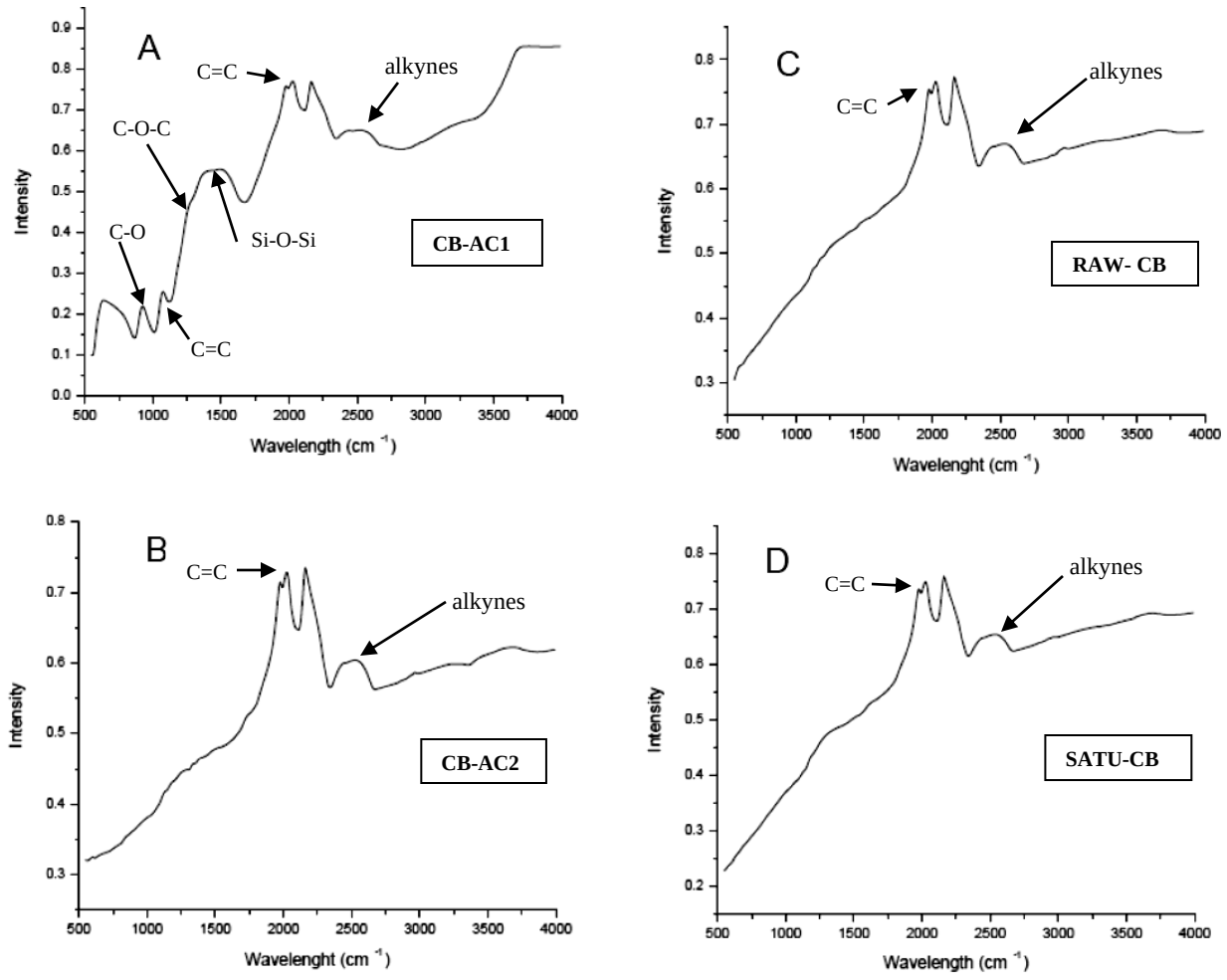

Fig 4.1: The FTIR spectra of carbonaceous materials (A) Activated by sulphuric acid (B) Activated by hydrogen peroxide (C) Raw carbon black (D) Saturated commercial activated carbon

4.2 Porosity Studies by BET analysis

The adsorbent porosity, pore diameter and surface areas are reported in Table 4.1. It is clear from these results that activated carbon prepared via impregnation with hydrogen peroxide exhibits high surface area, high micropore volume, and average pore volume diameter compared to the one activated by use of sulphuric acid. However, both activated carbons (CB-AC1 and CB-AC2) prepared via chemical activation in this study showed an improved surface area and micropore volume when compared to the raw pyrolytic carbon. The observed results can be attributed to effective percolation of the activating agents into the interior of the waste tyre carbon black. When this happens, the activating agent then breaks the lateral bonds in the cellulose molecules (increases *Inter* and *Intra* miscelle voids) influencing the surface properties (Dimpe et al., 2017).

In an independent study, (Sirimuangjinda et al. (2012) reported a surface area of 833 m^2/g for tyre waste-based activated carbon prepared via chemical treatment with H_3PO_4. The nitrogen sorption analysis results obtained confirmed the success of the chemical activation method and the influence of the chemical activating agents on the surface of carbon black. Based on the surface area and micropore volume results obtained, raw carbon black and the two as-prepared activated carbons were further used for the adsorption of Hg vapor. It has been reported that the uptake of a gaseous or liquid material by an adsorbent normally rely on the surface area and pore volume, which all indicate the degree of macroporosity in a carbonaceous material (Dimpe et al., 2017; Heo and Park, 2018).

Table 4.1: Nitrogen (N_2) sorption analysis results of adsorbents

Sample ID	**BJH Surface Area (m^2/g)**	**Micropore volume (cm^3/g)**	**BJH pore volume diameter (nm)**
RAW-CB	37.127	0.012	2.612
CB-AC 1	523.819	0.309	2.729
CB-AC 2	537.129	0.422	2.961
SATU-CB	33.931	0.031	2.393

4.3 Adsorbent Powder X-Ray Diffraction studies

The powder X-Ray Diffraction analysis was carried out on the adsorbents. The purpose was to evaluate the crystallinity, particle size, pore diameter and phase identification. The analysis was performed before and after activation. Raw pyrolytic carbon black as displayed in Figure 4.2 showed peaks at 2θ = 27 and 58º which correspond to the reflections from (111) and (222) planes for cubic ZnS. Additionally, peaks at 2θ = 51 and 64º which correspond to the reflections (102) and (110) planes, respectively, are of the wurtzite phase of ZnO. It has been reported that zinc oxides are normally added as vulcanization agents/catalysts during tyre manufacturing and these oxides decompose to different forms of ZnS during pyrolysis (Makam et al., 2018). However, as shown in Figure 4.2, the diffraction patterns depict broad bands centered around 2θ = 24, 25 and 45°, associated or attributed to (002), (100) and (101) planes, respectively (Omri and Benzina, 2012). These denote the stacking height Lc and the lateral size of the crystallites La in the carbonaceous material (Girgis et al., 2007). The presence of a predominantly porous structure,

especially in CB-AC2 (Fig. 4.2 D), is confirmed by the sharp peak around 2θ = 25º. The appearance of a sharp unknown or unidentified peak around 2θ =75° was observed by in their studies. It can also be noted that the diffraction patterns in CB-AC2 are relatively similar to the ones in the raw material, RAW-CB, except for a few peaks indicating an effective activation. Naturally, carbon black is a lignocellulosic material (containing interlinked cellulose, hemicellulose, and lignin structures). However, the introduction/use of an activant (i.e. H_2O_2) normally brings the breakdown and alteration of the 3D linkages between the chemical components of carbon black (cellulose, hemicellulose, lignin), thereby forming skeletons of fully disorganized carbonaceous materials (activated carbon). Furthermore, the X-ray diffraction patterns of saturated carbonaceous material SATU-CB, shows relatively broad, weak and low intensity peaks as compared to raw carbon black or H_2O_2-AC, confirming the interaction of carbonaceous material with adsorbate. In comparison, Makam et al. (2018) also studied the crystallographic structure of activated carbon prepared via KOH activation. A broad hump peak was observed around 2θ = 22º, which was attributed to the amorphous nature of the carbon material before activation. After KOH treatment, sharp peaks around 2θ = 23º were observed and assigned to the turbostratic structure and corresponds to the (002) reflection. From the pXRD diffractions pattens shown in Figure 4.2 it can be concluded that the raw pyrolytic carbon black and the hydrogen peroxide activated carbon black are more crystalline (sharp peaks) and the commercial grade activated carbon was found to be more amorphous (blund peaks).

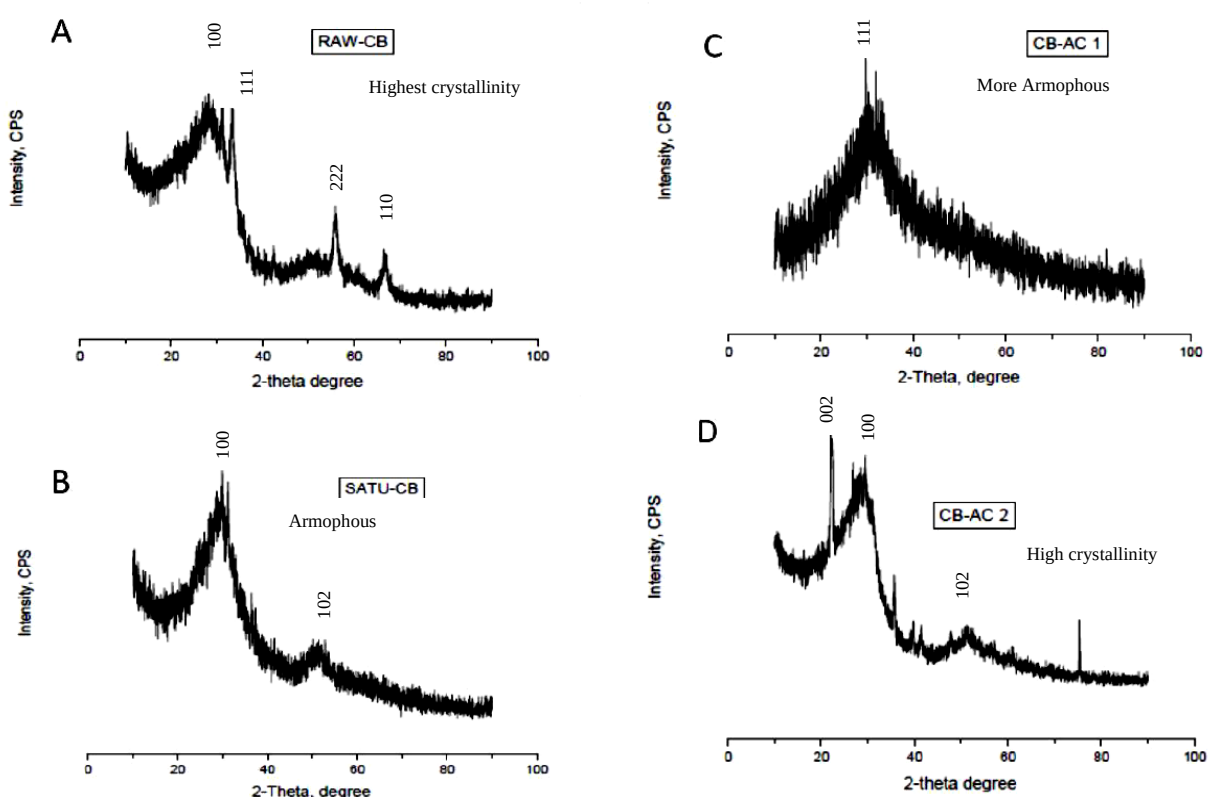

Fig 4.2: Powder XRD patterns of adsorbents (A) Raw carbon black (B) Saturated commercial activated carbon (C) Activated by sulphuric acid (D) Activated by hydrogen peroxide

4.4 Outputs from SEM/EDX Analysis

The Scanning Electron Microscope analysis was carried out to understand the sample surface topography. The sample chemical composition, including what elements are present as well as their distribution and concentration were detected by EDX coupled to SEM. The surface morphology and elemental content of the sample was achieved by coupling the SEM with energy-dispersive X-ray spectroscopy SEM/EDX). The instrument settings especially the magnification was adjusted differently for each sample. This was done to select the best visual images for presentation of the results. These different magnifications are clearly marked on the figures.

4.4.1 Raw pyrolytic carbon

The results are displayed in Fig 4.3. It is evident that raw carbon black exhibits (Fig 4.3 (A)) a dense and rough porous structure with very limited pores. The EDX result confirms a high carbon content and minimal presence of other elements such as sodium (Na), silicon (Si) and sulfur (S) in raw carbon black.

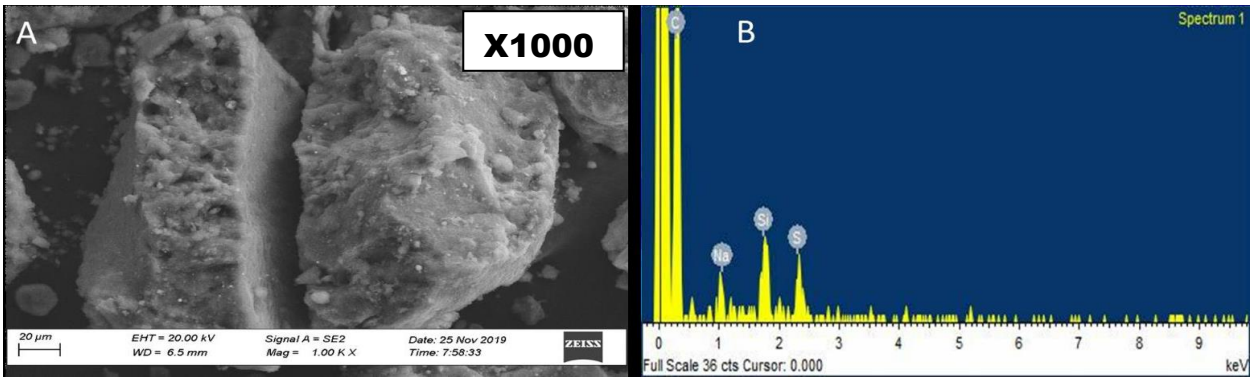

Fig 4.3: SEM/EDX of raw pyrolytic carbon black

The advantage of scanning electron microscope (SEM) is that, it shows both micro- and mesoporous structures of carbonaceous materials. Furthermore, the backscatter electron technique was applied to further analyze the surface of the materials against Hg. Light and heavy Hg was seen and confirmed by EDX analysis (Fig. 4.4 C-D, respectively). Hg is known to show dense and lighter spots when screened by the backscatter electrons. In the study by Musmarra et al. (2016) it was revealed through the SEM/EDX analysis that high elementary Hg vapor concentration was found in synchronicity with high sulfur content in an Hg-saturated carbon material as very white spots in the SEM images (Musmarra et al., 2016). In this study, it can be concluded that the interactions between Hg and the activated carbons were influenced and facilitated by heterogeneous surface (oxygen-functionalities) of the adsorbent and its narrow micropores. Due to the heterogeneous surface nature of the activated carbons and varying number of oxygen-functionalities, the adsorption of Hg is believed to have involved both the physisorption and chemisorption valence forces in both multilayer and monolayer fashion (Ruiz et al., 2010).

4.4.2 Commercial activated carbon

After adsorption it was expected that some Hg will be spotted and noticed on the surface of the activated carbon. As shown in Fig. 4.4 (A and B), the surface of the activated carbon is covered by dense and light Hg depositions. To that effect, the light spots of Hg infused in the pores of the activated carbon were also deeply checked and focused with high resolution of the microscopy and EDX (Fig. 4.4C). Fig. 4.4 (A and B) illustrates the round-ball like structure of Hg found inside the pores of the activated carbons.

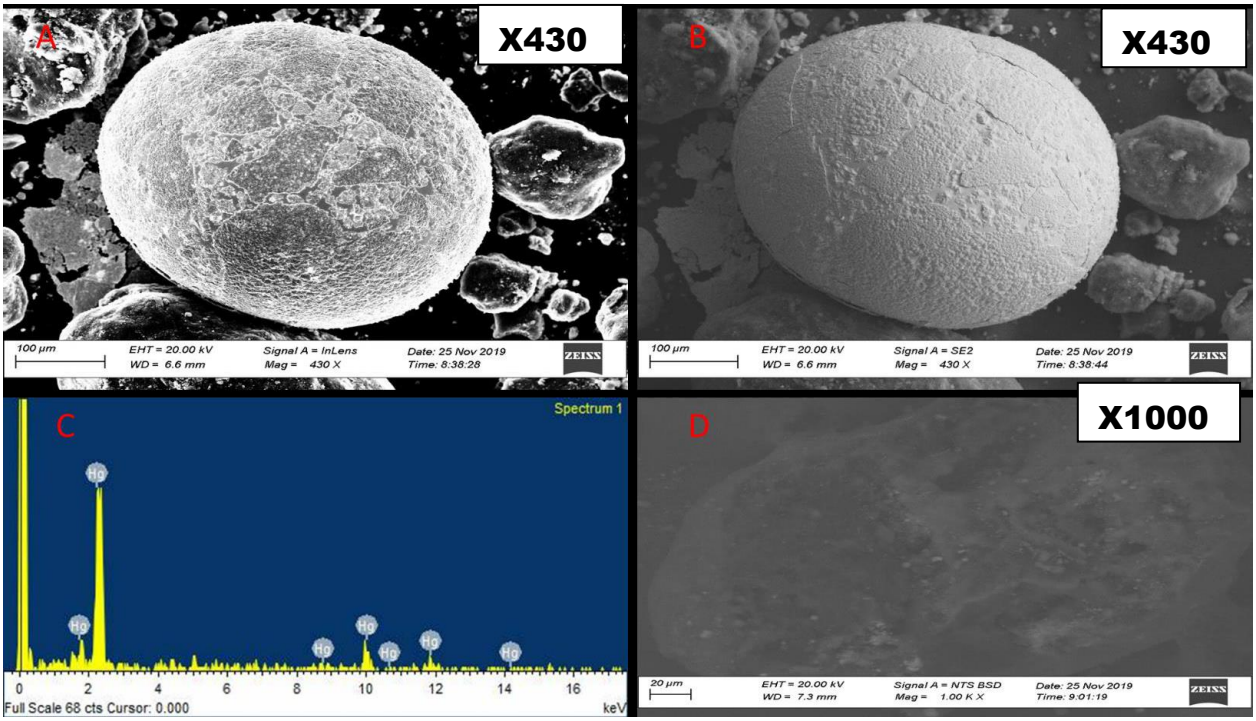

Fig 4.4: SEM/EDX of SATU-CB (A) SEM before desorption (B) partly desorbed (C) EDX before desorption (D) SEM after complete desorption

4.4.2 Sulphuric acid activated carbon

Upon activation with sulphuric acid, the SEM/EDX images are shown in Fig 4.5. These images show a more porous adsorbent when compared to those of saturated carbon and the raw pyrolytic carbon. However, the sulphuric acid activated product appears to be less porous than the hydrogen peroxide activated one. This qualitative assessment trend of results is further confirmed by the BET results reported in Table 4.1. Based on these observations it is likely that sulphuric acid activated tyre pyrolytic carbon will adsorb less effectively than its hydrogen peroxide activated counterpart but far much better than the SATU-CB and the RAW-CB.

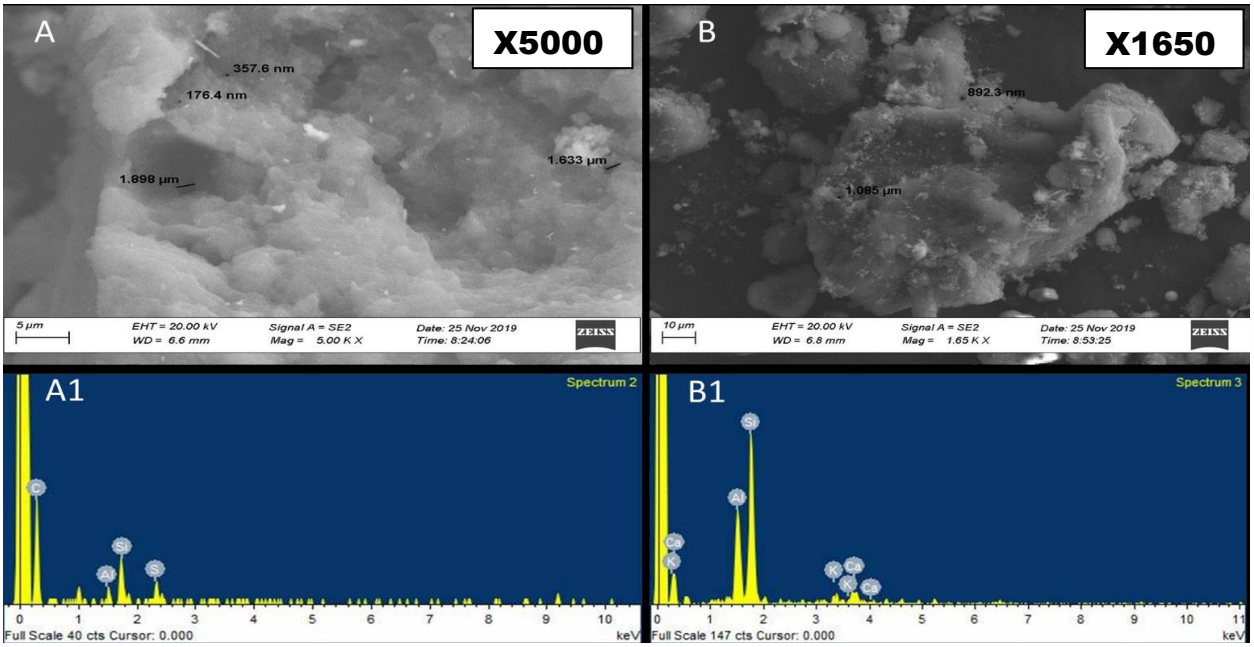

Fig 4.5 SEM/EDX of CB-AC1 before (A/A1) and after (B/B1) adsorption of Hg

4.4.3 Hydrogen peroxide activated

The SEM/EDX images displayed in Fig 4.6 were derived from carbon activated by hydrogen peroxide activation. The surface morphology of the resultant activated carbon is dominated by increased and improved irregular cracks and pores with many shapes and sizes. Dimpe et al. (2017) observed similar images when they prepared their own activated carbon from waste tyres as well. This type of porous morphology confirms that activation with hydrogen peroxide was successful and it produced carbonaceous material with improved porous structure (as shown in the BET analysis).

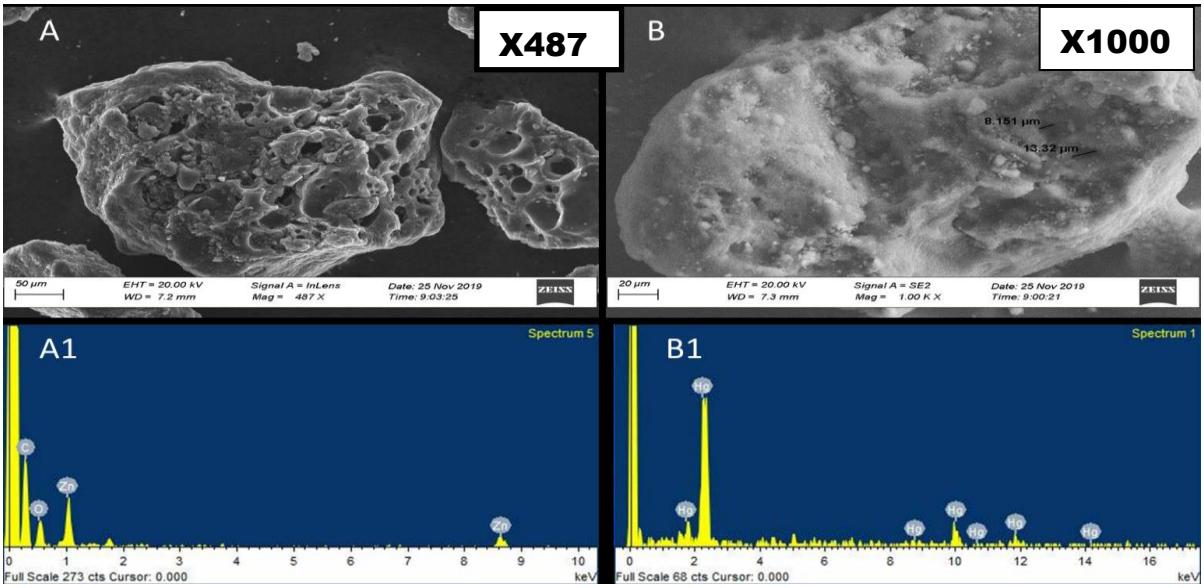

Fig 4.6: SEM/EDX of CB-AC2 before (A/A1) and after (B/B1) adsorption of Hg

4.5 Mercury Recovery by Adsorption

The mercury adsorbed on tested adsorbents during the adsorption trials was calculated by a simple mass balance approach. In this approach the difference between adsorbent weights before and after adsorption represented the mercury weight adsorbed. The measurement of weight for the adsorbents before and after adsorption is depicted in Fig 4.7.

Fig 4.7: Analytical balance weighing adsorbent

The said mass balance principle is applicable because only pure mercury vapours were allowed to pass through the 54.8 grammes (g) of adsorbent loaded into the reactor and therefore no other thing could increase its weight besides the adsorbing mercury. The small variation between the initially loaded mercury (4.89 g) and the calculated adsorbed mercury represents mercury that was lost to the atmosphere. These results are depicted in Table 4.2. Tyre pyrolytic carbon activated by hydrogen peroxide recovered 92% of the vaporised mercury while the sulphuric acid activated carbon had a lesser mercury recovery capacity at 90%. This matches with predictions made based on the characterisation of these two adsorbents. Pore sizes and surface areas on the adsorbents were higher for hydrogen peroxide versus sulphuric acid activated carbon. These mercury recoveries are compared to those established by other authors using corn based activated carbon although under optimised conditions they could record as high as 99% mercury recoveries (Duan et al., 2019)

Table 4.2 Mercury weight adsorbing on test materials

Adsorbent	Adsorbent loaded (g)	Adsorbent weight after adsorption (g)	Mercury adsorbed (g)	Mercury recovery (%)
CB-AC1	54.8	59.2	4.4	90.0
CB-AC2	54.8	59.3	4.5	92.0

4.6 Chapter Conclusions

A comparison of the SEM images of the adsorbents indicate that the commercial grade activated carbon (SATU-CB) has the highest surface area (micropores) among the adsorbents. This was contrary to nitrogen sorption results displayed in Table 4.1 because the BET analysis was performed on a saturated (already exhausted) commercial adsorbent whose pores were blocked by the adsorbate. For the prepared adsorbents, the nitrogen sorption results apply to freshly unused products. The SEM images discussed in the current section, however, were derived from SATU-CB that had undergone desorption. The desorbed SATU-CB with active sites therefore showed a higher surface area than the newly tyre based activated carbons according to SEM technique. This was followed by the hydrogen peroxide activated carbon (CB-AC2) and lastly the sulphuric acid activated carbon (CB-AC1). Because of these variations in surface area properties, the CB-AC2 adsorbed Hg slightly better (92%) than CB-AC1 (90%).

Comparing the XRD analysis of the above activated carbons showed that the commercial grade sample had very few broad-weak peaks, signifying disturbed or altered crystalline structure than

the raw carbon black and the activated ones (Fig 4.2). The activation of the pyrolytic waste tyre carbon black with hydrogen peroxide solution was found to improve the adsorption capacity as denoted by the increase in surface area, and therefore its performance for Hg adsorption. The improvement in the removal efficiency was attributed to the increase of the breakdown and alteration of the 3D linkages between the chemical components of carbon black (cellulose, hemicellulose, lignin) by the chemical activants, thereby forming skeletons of fully disorganized carbonaceous materials (Girgis et al., 2007). Activated carbon black materials produced via the chemical activation method were observed to have high surface areas and well-developed pore structures.

CHAPTER FIVE: CONCLUSIONS AND RECOMMENDATIONS

5.1 Answers to Research Questions

Research questions formulated for this research are separately answered below.

i. **Can a mercury vapor adsorbent be prepared from the carbonaceous residue of waste tyre pyrolysis?**

   From the IR analytical spectrum of raw pyrolytic carbon black, it was observed that the pyrolytic carbon black does exhibits some functional groups though very little as compared to the hydrogen peroxide (H_2SO_4-AC) and the sulphuric acid activated H_2O_2-AC carbonaceous materials prepared. Furthermore, the FTIR analysis of the raw pyrolytic carbonaceous materials showed a carbon double bond (C=C) stretching vibration attributed to the lignocellulose aromatic ring at 1657-2000 cm^{-1}. This was an indicator of the carbonaceous material displaying potential qualities to be further developed into a Hg adsorbent activated carbon.

ii. **How does tyres pyrolytic carbonaceous material derived adsorbent compare to the current industry adopted mercury vapour adsorbents?**

   The surface morphology investigation of the pyrolytic carbonaceous materials using SEM (under secondary and backscatter electrons) and EDX revealed that the porous morphology of activated carbons activated by hydrogen peroxide produced carbonaceous material with improved porous structure and was complimented by BET analysis results obtained. However, after adsorption it was expected that some Hg will be spotted and noticed on the surface of the activated carbon. Furthermore, the backscatter electron analysis was employed and round-ball like structures of Hg were found inside the pores of the activated carbons. Additionally, light and heavy Hg was seen and confirmed by EDX analysis.

iii. **Could the choice of activation agent matter in the preparation of mercury adsorbent from tyre pyrolytic residues?**

   The results from the BET analysis confirmed the effectiveness of the chemical activation method and the influence of the chemical agents on the surface of carbon black. This was

demonstrated by the drastic increase on surface areas and micropore volumes of the chemically activated pyrolytic carbon black by over fourteen times for the hydrogen peroxide (537.129 m^2/g) and sulphuric acid (523.819 m^2/g) activated carbonaceous residues against the raw pyrolytic carbon black (37.127 m^2/g). Hydrogen peroxide proved to be superior than sulphuric acid in activating tyre based carbon black for use as adsorbent. The mercury recoveries of 92% when using hydrogen peroxide activated carbon and 90% for sulphuric acid activated carbon further verifies the superiority of the former activating agent.

5.2 Research Conclusions

The experimental work done on the chemical preparation, characterization and performance evaluation of pyrolytic carbon black and its as-prepared activated carbons presented it as a potential adsorbent for Hg vapour (Hg) recovery. The FTIR, BET, SEM/EDX and pXRD analytical techniques were employed to elucidate the physiochemical properties of the adsorbents. The observed mercury-carbon interactions could have been influenced and facilitated by heterogeneous surface (oxygen-functionalities) of the adsorbent and its narrow micropores. Adsorption potentially proceeded by both the physisorption and chemisorption forces through both multilayer and monolayer fashion. The SEM images showed mercury balls in pores. Also, after adsorption trials, EDX revealed mercury peaks demonstrating that mercury adsorption had taken place on the adsorbent. Therefore, tyre pyrolysis-based carbon black can be prepared into activated carbon with potential for its use as mercury adsorbent. The current adsorption potential demonstrated by this tyre based carbon is slightly lower to that of commercially available activated carbon.

5.3 Research Recommendations

- There is a need to further study the chemistry of the pyrolytic carbon black and its interaction with various activation agents extensively. This will help in understanding the underlying properties and parameters that contribute towards commercialization of this potential product.
- Although, observations made in this study by analysis of SEM images and EDX results confirm that tyre pyrolysis based activated carbons can adsorb Hg , further qualitative

and quantitative investigations are still necessary to optimize this possible solution and acquire an in-depth know-how around application of this solution.

- It may also be prudent to investigate the nature (vapor or liquid) and the chemical behavior of Hg inside or on the surface of the adsorbents. This is triggered by the difficult to explain presence of round-ball like structure of Hg found inside the pores of the activated carbon. There is a possibility that the Hg vapor adsorbed by the carbonaceous is converted to liquid form when subjected or screened by high-temperature SEM gun-beam.

REFERENCES

Abai, M., Atkins, M.P., Hassan, A., Holbrey, J.D., Kuah, Y., Nockemann, P., Oliferenko, A.A., Plechkova, N. V., Rafeen, S., Rahman, A.A., Ramli, R., Shariff, S.M., Seddon, K.R., Srinivasan, G., Zou, Y., 2015. An ionic liquid process for mercury removal from natural gas. Dalt. Trans. 44, 8617–8624. https://doi.org/10.1039/c4dt03273j

Adelodun, A.A., Lim, Y.H., Jo, Y.M., 2014. Surface oxidation of activated carbon pellets by hydrogen peroxide for preparation of CO2 adsorbent. J. Ind. Eng. Chem. 20, 2130–2137.

Bamdad, H., Hawboldt, K., MacQuarrie, S., 2018. A review on common adsorbents for acid gases removal: Focus on biochar. Renew. Sustain. Energy Rev. 81, 1705–1720. https://doi.org/10.1016/j.rser.2017.05.261

Beckers, F., Rinklebe, J., 2017. Cycling of mercury in the environment: Sources, fate, and human health implications: A review. Crit. Rev. Environ. Sci. Technol. 47, 693–794. https://doi.org/10.1080/10643389.2017.1326277

Birkner, N., Wang, Q., 2020. How an FTIR spectrometer operates. Chemistry (Easton). 1–7.

Bob, U., Padayachee, A., Gordon, M., Moutlana, I., 2017. Enhancing innovation and technological case study of South African government sector. Sci. Technol. Sci. 2, 332–349. https://doi.org/10.1177/0971721817702293

Carmalin, S.A., Lima, E.C., 2018. Removal of emerging contaminants from the environment by adsorption. Ecotoxicol. Environ. Saf. 150, 1–17. https://doi.org/10.1016/j.ecoenv.2017.12.026

Carocci, A., Rovito, N., Sinicropi, M., Genchi, G., 2014. Mercury toxicity and neurodegenerative effects, in: Whitacre, D. (Ed.), Reviews of Environmental Contamination and Toxicology. Springer, Cham, pp. 1–18. https://doi.org/https://doi.org/10.1007/978-3-319-03777-6_1

Choi, Y., Choi, H.J., Rhee, S.W., 2020. Estimation on hazardous characteristics of the components from linear type of end-of-life light-emitting diode lamps. J. Mater. Cycles Waste Manag. 22, 307–314. https://doi.org/10.1007/s10163-019-00913-6

Christian, M.S., Otero-de-la-Roza, A., Johnson, E.R., 2017. Adsorption of graphene to metal (111) surfaces using the exchange-hole dipole moment model. Carbon. 124, 531–540. https://doi.org/10.1016/j.carbon.2017.08.077

Coasne, B., Farrusseng, D., 2019. Microporous and mesoporous materials gas oversolubility in nanoconfined liquids : Review and perspectives for adsorbent design. Microporous Mesoporous Mater. 288, 109561–109569.

Crini, G., Lichtfouse, E., Wilson, L.D., Morin-Crini, N., 2019. Conventional and non-conventional adsorbents for wastewater treatment. Environ. Chem. Lett. 17, 195–213. https://doi.org/10.1007/s10311-018-0786-8

Daniel, J., Cardona-uribe, N., Murillo, R., García, T., Manuel, J., 2019. Carbon black recovery from waste tire pyrolysis by demineralization: Production and application in rubber compounding 85, 574–584.

Dimpe, K.M., Ngila, J.C., Nomngongo, P.N., 2017. Application of waste tyre-based activated carbon for the removal of heavy metals in wastewater. Cogent Eng. 4, 1–11. https://doi.org/10.1080/23311916.2017.1330912

Djilani, C., Zaghdoudi, R., Djazi, F., Bouchekima, B., Lallam, A., Modarressi, A., Rogalski, M., 2015. Adsorption of dyes on activated carbon prepared from apricot stones and commercial activated carbon. J. Taiwan Inst. Chem. Eng. 53, 112–121.

Xue-Lei, Duan., Chun-Gang, Yuan., Tian-Tian, Jing., Xiao-Dong, Yuan., 2019. Removal of elemental mercury using large surface area micro-porous corn
cob activated carbon by zinc chloride activation. Fuel. 239, 830–840. https://doi.org/10.1016/j.fuel.2018.11.017

Duncan, T., 2019. What is flourescent lighting?. Online document. Blog. URL https://insights.regencylighting.com/what-is-fluorescent-lighting (accessed 11.29.19).

Eskom, 2019. Tariff history. Online document. URL http://www.eskom.co.za/CustomerCare/TariffsAndCharges/Pages/Tariff_History.aspx (accessed 11.15.19).

Eskom, 2013. CFL recovery, recycling & disposal implementation guideline. Online document. URL www.eskom.co.za%3Eidm%3E1280ESKD_CFL-Brochure (accessed 11.13.19).

Ghosh, Sadhan Kumar, Debnath, B., Baidya, R., De, D., Li, J., Ghosh, Sannidhya Kumar, Zheng, L., Awasthi, A.K., Liubarskaia, M.A., Ogola, J.S., Tavares, A.N., 2016. Waste electrical and electronic equipment management and Basel Convention compliance in Brazil, Russia, India, China and South Africa (BRICS) nations. Waste Manag. Res. 34, 693–707. https://doi.org/10.1177/0734242X16652956

Gichuki, S.W., Mason, R.P., 2013. Mercury and metals in South African precipitation. Atmos. Environ. 79, 286–298. https://doi.org/10.1016/j.atmosenv.2013.04.009

Girgis, B.S., Temerk, Y.M., Gadelrab, M.M., Abdullah, I.D., 2007. X-ray Diffraction patterns of activated carbons prepared under various conditions. Carbon Lett. 8, 95–100. https://doi.org/10.5714/cl.2007.8.2.095

Heo, Y.-J., Park, S.-J., 2018. H_2O_2/steam activation as an eco-friendly and efficient top-down approach to enhancing porosity on carbonaceous materials: The effect of inevitable oxygen functionalities on CO_2 capture. Green Chem. 20, 5224–5234. https://doi.org/10.1039/c8gc02570c

Ho, T.C., Lee, Y., Chu, H.W., Lin, C.J., Hopper, J.R., 2005. Modeling of mercury desorption from activated carbon at elevated temperatures under fluidized/fixed bed operations. Powder Technol. 151, 54–60. https://doi.org/10.1016/j.powtec.2004.11.034

Honda, S., Hylander, L., Sakamoto, M., 2006. Recent advances in evaluation of health effects on mercury with special reference to methylmercury – A Minireview. Environ. Health Prev.

Med. 11, 171–176.

Horowitz, H.M., Jacob, D.J., Amos, H.M., Streets, D.G., Sunderland, E.M., 2014. Historical mercury releases from commercial products: Global environmental implications. Environ. Sci. Technol. 48, 10242–10250. https://doi.org/10.1021/es501337j

Jampaiah, D., Ippolito, S.J., Sabri, Y.M., Tardio, J., Selvakannan, P.R., Nafady, A., Reddy, B.M., Bhargava, S.K., 2016. Ceria-zirconia modified MnOx catalysts for gaseous elemental mercury oxidation and adsorption. Catal. Sci. Technol. 6, 1792–1803. https://doi.org/10.1039/c5cy01534k

Jawad, A.H., Rashid, R.A., Azlan, M., Ishak, M., Wilson, L.D., Jawad, A.H., Rashid, R.A., Azlan, M., Ishak, M., Wilson, L.D., 2016. Adsorption of methylene blue onto activated carbon developed from biomass waste by H_2SO_4 activation: kinetic, equilibrium and thermodynamic studies. Desalin. Water Treat. 57, 25194–25206. https://doi.org/10.1080/19443994.2016.1144534

Kawai, S., Foster, A.S., Meyer, E., Canova, F.F., Gade, L.H., Jung, T.A., 2016. Van der Waals interactions and the limits of isolated atom models at interfaces. Nat. Commun. 7, 1–7. https://doi.org/10.1038/ncomms11559

Kim, K.-H., Kabir, E., Jahan, S.A., 2016. A review on the distribution of Hg in the environment and its human health impacts. J. Hazard. Mater. 310, 278–279. https://doi.org/10.1016/j.jhazmat.2016.02.043

Liu, H., Zhao, Y., Zhou, Y., Chang, L., Zhang, J., 2019. Removal of gaseous elemental mercury by modified diatomite. Sci. Total Environ. 652, 651–659. https://doi.org/10.1016/j.scitotenv.2018.10.291

Lohren, H., Bornhorst, J., Galla, H.J., Schwerdtle, T., 2015. The blood-cerebrospinal fluid barrier - first evidence for an active transport of organic mercury compounds out of the brain. Metallomics 7, 1420–1430. https://doi.org/10.1039/c5mt00171d

Lu, X., Jiang, J., Sun, K., Wang, J., Zhang, Y., 2014. Influence of the pore structure and surface chemical properties of activated carbon on the adsorption of mercury from aqueous solutions. Mar. Pollut. Bull. 78, 69–76.

Lydall, M., Nyanjowa, W., James, Y., 2017. Mapping South Africa's waste electrical and electronic equipment (WEEE) dismantling, pre-processing and processing technology landscape. Waste Research Development and Innovation Roadmap Research Report. Mintek pp 91

Makam, P., Shilpa, R., Kandjani, A.E., Periasamy, S.R., Sabri, Y.M., Madhu, C., Bhargava, S.K., Govindaraju, T., 2018. SERS and fluorescence-based ultrasensitive detection of mercury in water. Biosens. Bioelectron. 100, 556–564. https://doi.org/10.1016/j.bios.2017.09.051

Maqbool, F., Niaz, K., Hassan, F.I., Khan, F., Abdollahi, M., 2017. Immunotoxicity of mercury: Pathological and toxicological effects. J. Environ. Sci. Heal. - Part C Environ. Carcinog. Ecotoxicol. Rev. 35, 29–46. https://doi.org/10.1080/10590501.2016.1278299

Maroneze, M.M., Zepka, L.Q., Vieira, J.G., Queiroz, M.I., Jacob-Lopes, E., 2014. A tecnologia de remoção de fósforo: Gerenciamento do elemento em resíduos industriais. Rev. Ambient. e Agua 9, 445–458. https://doi.org/10.4136/1980-993X

Matandabuzo, M., Ajibade, P.A., 2018. Removal of metal ions from aqueous solutions using activated carbon prepared from *Zea mays* stem. Sci. Study Res. 19, 117–132.

Moerz, S.T., Huber, P., 2014. Protein adsorption into mesopores: a combination of electrostatic interaction, counter ion release, and Van der Waals forces. Langmuir 30, 2729–2737. https://doi.org/10.1021/la404947j

Monteillet, H., Workamp, M., Appel, J., Kleijn, J.M., Leermakers, F.A.M., Sprakel, J., 2014. Ultrastrong anchoring yet barrier-free adsorption of composite microgels at liquid interfaces. Adv. Mater. Interfaces 1, 1–9. https://doi.org/10.1002/admi.201300121

Mukosha, L., Onyango, M.S., Ochieng, A., Kasaini, H., 2013. Development of better quality low-cost activated carbon from South African pine tree (*pinus patula*) sawdust: characterization and comparative phenol adsorption. Int. J. Chem. Mol. Eng. 27, 546–556.

Musmarra, D., Karatza, D., Lancia, A., Prisciandaro, M., Mazziotti di Celso, G., 2016. Adsorption of elemental mercury vapors from synthetic exhaust combustion gas onto HGR carbon. J. Air Waste Manag. Assoc. 66, 698–706. https://doi.org/10.1080/10962247.2016.1170077

Navarro, A., Cañadas, I., Rodríguez, J., 2014. Thermal treatment of mercury mine wastes using a rotary solar kiln. Minerals 4, 37–51. https://doi.org/10.3390/min4010037

Nguyen, H., You, S., Chao, H., 2016. Thermodynamic parameters of cadmium adsorption onto orange peel calculated from various methods : A comparison study. J. Environ. Chem. Eng. 4, 2671–2682.

Omri, A., Benzina, M., 2012. Characterization of activated carbon prepared from a new raw lignocellulosic material*: Ziziphus spina-christi* seeds. J. la Société Chim. Tunisie 14, 175–183.

Oyekale, A.S., 2015. Factors explaining households ' cash payment for solid waste disposal and recycling behaviors in south africa. Sustainability 7, 15882–15899. https://doi.org/10.3390/su71215795

Panchia, J., Krige, Y., 2020. Amid lockdown, South Africa's waste pickers suffer most. Online material. Aljazeera News South Africa. URL https://www.aljazeera.com/news/2020/04/lockdown-south-africa-waste-pickers-suffer-200408113458382.html#:~:text=While there is no official,Africa between 60%2C000 and 90%2C000. (accessed 4.8.20).

Particle Analytical, 2019. Introduction to BET (Brunauer, Emmett and Teller) Online material. URL https://particle.dk/methods-analytical-laboratory/surface-area-bet-2/ (accessed 1.7.20).

Pietrzak, R., Nowicki, P., Kaźmierczak, J., Kuszyńska, I., Goscianska, J., Przepiórski, J., 2014. Comparison of the effects of different chemical activation methods on properties of carbonaceous adsorbents obtained from cherry stones. Chem. Eng. Res. Des. 92, 1187–

1191. https://doi.org/10.1016/j.cherd.2013.10.005

Pilusa, J., Muzenda, E., 2013. Beneficiation of pyrolitic carbon black. Int. J. Chem. Nucl. Mater. Metall. Eng. 7, 392–396.

Pilusa, J., Shukla, M., Muzenda, E., 2014. Economic Assessment of Waste Tyres Pyrolysis Technology : A Case study for Gauteng Province, South Africa. Int. J. Res. Chem. Metall. Civ. Eng. 1, 41–49.

Ponec, V., Knor, Z., Cerny, S., 2018. Adsorption on Solids. Butterworth.

Puty, B., Ketlen, L., Leão, R., Crespo-lopez, M.E., Paula, A., Ponte, C., Carvalho, S., Carolina, N., Fagundes, F., Cople, L., Rodrigues, R., 2019. Association between methylmercury environmental exposure and neurological disorders: A systematic review. J. Trace Elem. Med. Biol. 52, 100–110.

Reclite, 2019. Process. Online material. URL https://www.reclite.co.za/process/ (accessed 12.5.19).

Recor, 2019. Waste tyres to electricity. Online material. Web news. URL https://www.recor.co.za/tyre-pyrolysis (accessed 11.21.19).

Rhee, S., Park, H., Choi, H., 2015. Comparison of mercury distribution between the types of spent fluorescent lamp. Arch. Metall. Mater. 60, 3–5. https://doi.org/10.1515/amm-2015-0117

Ringwood, F., 2015. Bettering home energy use-: human settlements. IMIESA 40, 26–29.

Ruiz, B., Cabrita, I., Mestre, A.S., Parra, J.B., Pires, J., Carvalho, A.P., Ania, C.O., 2010. Surface heterogeneity effects of activated carbons on the kinetics of paracetamol removal from aqueous solution. Appl. Surf. Sci. 256, 5171–5175. https://doi.org/10.1016/j.apsusc.2009.12.086

Schröder, P., 2017. Compliant waste management for lighting, fittings and electronic components. Online document. Articles. URL https://www.ee.co.za/article/compliant-waste-management-lighting-fittings-electronic-components.html (accessed 11.24.19).

Shang, H., Lu, Y., Zhao, F., Chao, C., 2015. Preparing high surface area porous carbon from biomass by carbonization in a molten salt medium. RSC Adv. 5, 75728–75734. https://doi.org/10.1039/c5ra12406a

Singh, L.P., Katal, G., 2013. A comparative study on design and operation of fluorescent lamps, CFLs and LEDs. J. Eng. Res. Appl. 3, 401–407.

Sirimuangjinda, A., Hemra, K., Atong, D., Pechyen, C., 2012. Production and characterization of activated carbon from waste tire by H_3PO_4 treatment for ethylene adsorbent used in active packaging. Adv. Mater. Res. 506, 214–217. https://doi.org/10.4028/www.scientific.net/AMR.506.214

Song, X., Wang, L., Gong, J., Zhan, X., Zeng, Y., 2020. Exploring in new method to study the effects of surface functional groups on adsorption of CO2 and CH_4 on activated carbons

adsorption of CO_2 and CH_4 on activated carbons. Langmuir 36, 3862–3870. https://doi.org/10.1021/acs.langmuir.9b03475

Stoquart, C., Barbeau, B., Servais, P., Vázquez-Rodríguez, G.A., 2014. Quantifying bacterial biomass fixed onto biological activated carbon (PAC and GAC) used in drinking water treatment. J. Water Supply Res. Technol. - AQUA 63, 1–11. https://doi.org/10.2166/aqua.2013.101

Sun, P., Zhang, B., Zeng, X., Luo, G., Li, X., Yao, H., Zheng, C., 2017. Deep study on effects of activated carbon ' s oxygen functional groups for elemental mercury adsorption using temperature programmed desorption method. Fuel 200, 100–106.

Tan, Q., Li, J., 2016. Potential mercury emissions from fluorescent lamps production and obsolescence in mainland China. Waste Manag. Res. 34, 67–74. https://doi.org/10.1177/0734242X15616473

Tao, J., Rappe, A.M., 2014. Physical Adsorption: Theory of Van der Waals interactions between particles and clean surfaces. Phys. Rev. Lett. 112, 1–5. https://doi.org/10.1103/PhysRevLett.112.106101

Tiedemann, K., Freeman, L., Bredenkamp, B., 2004. Impacts of the South African efficient lighting initiative, in: Domestic Use of Energy Conference. pp. 1–7.

Tonigold, K., Groß, A., 2010. Adsorption of small aromatic molecules on the (111) surfaces of noble metals: A density functional theory study with semiempirical corrections for dispersion effects. J. Chem. Phys. 132. https://doi.org/10.1063/1.3439691

Tran, H.N., You, S.-J., Hosseini-Bandegharaei, A., Chao, H.-P., 2017. Mistakes and inconsistencies regarding adsorption of contaminants from aqueous solutions_ A critical review. Water Res. 120, 88–116.

Tunsu, C., Ekberg, C., Retegan, T., 2014. Characterization and leaching of real fluorescent lamp waste for the recovery of rare earth metals and mercury. Hydrometallurgy 144–145, 91–98. https://doi.org/10.1016/j.hydromet.2014.01.019

Venter, L., 2008. Recovery of compact fluorescent lamps from the general household waste stream.

Wang, M., Zhang, L., Li, A., Irfan, M., Du, Y., Di, W., 2019. Comparative pyrolysis behaviors of tire tread and side wall from waste tire and characterization of the resulting chars. J. Environ. Manage. 232, 364–371.

Williams, P.T., 2013. Pyrolysis of waste tyres : A review. Waste Manag. 33, 1714–1728.

Wilson, E., Lafferty, J.S., Thiboldeaux, R., Tomasallo, C., Grajewski, B., Wozniak, R., Meiman, J., 2018. Occupational mercury exposure at a fluorescent lamp recycling facility-Wisconsin, 2017. Morb. Mortal. Wkly. Rep. 67, 763–766. https://doi.org/10.15585/mmwr.mm6727a3

Wu, Y., Yin, X., Zhang, Q., Wang, W., Mu, X., 2014. The recycling of rare earths from waste tricolor phosphors in fluorescent lamps: A review of processes and technologies. Resour.

Conserv. Recycl. 88, 21–31. https://doi.org/10.1016/j.resconrec.2014.04.007

Xia, Z., Meijerink, A., 2017. Ce^{3+}-doped garnet phosphors: composition modification, luminescence properties and applications. Chem. Soc. Rev. 46, 275–299. https://doi.org/10.1039/c6cs00551a

Xu, W., Pan, J., Fan, B., Liu, Y., 2019. Removal of gaseous elemental mercury using seaweed chars impregnated by NH_4Cl and NH_4Br. J. Clean. Prod. 216, 277–287. https://doi.org/10.1016/j.jclepro.2019.01.195

Ynalvez, R., Gutierrez, J., Gonzalez-Cantu, H., 2016. Mini-review: toxicity of mercury as a consequence of enzyme alteration. BioMetals 29, 781–788. https://doi.org/10.1007/s10534-016-9967-8

Yorifuji, T., Tsuda, T., 2016. Epidemiological studies of neurological signs and symptoms and blood pressure in populations near the industrial methylmercury contamination at Minamata, Japan. Arch. Environ. Occup. Heal. 17, 231–236. https://doi.org/10.1080/19338244.2015.1084261

Yoshida, S., Matsumoto, S., Kanchika, T., Hagiwara, T., Minami, T., 2016. The organic mercury compounds, methylmercury and ethylmercury, inhibited ciliary movement of ventricular ependymal cells in the mouse brain around the concentrations reported for human poisoning. Neurotoxicology 57, 69–74. https://doi.org/10.1016/j.neuro.2016.08.007